Wireless Netw
DOI 10.1007/s11276-007-0092-z

Detection of mobile targets on the plane and in space using heterogeneous sensor networks

Loukas Lazos · Radha Poovendran · James A. Ritcey

Abstract Detection of targets moving within a field of interest is a fundamental service Wireless Sensor Network (WSN) service. The WSN's target detection performance is directly related to the placement of the sensors within the field of interest. In this paper, we address the problem of deterministic sensor deployment on the plane and in space, for the purpose of detecting mobile targets. We map the target detection problem to a line-set intersection problem and derive analytic expressions for the probability of detecting mobile targets. Compared to previous works, our mapping allows us to consider sensors with heterogeneous sensing capabilities, thus analyzing sensor networks that employ multiple sensing modalities. We show that the complexity of evaluating the target detection probability grows exponentially with the network size and, hence, derive appropriate lower and upper bounds. We also show that maximizing the lower bound on the probability for target detection on the plane and in space, is analogous to the problem of minimizing the average symbol error probability in two-dimensional and three-dimensional digital modulation schemes, respectively, over additive white Gaussian noise. These problems can be addressed using the circle packing problem for the plane, and the sphere packing problem for space. Using the analogy to digital modulation schemes, we derive sensor constellations from well known signal constellations with low average symbol error probability.

Keywords Target detection · WSN · Heterogeneous · Space · Plane

L. Lazos (✉)
Department of Electrical and Computer Engineering,
University of Arizona, Tucson, AZ, USA
e-mail: llazos@ece.arizona.edu

R. Poovendran
Network Security Lab (NSL), University of Washington,
Seattle, WA, USA
e-mail: rp3@u.washington.edu

J. A. Ritcey
Department of Electrical Engineering,
University of Washington, Seattle, WA, USA
e-mail: ritcey@ee.washington.edu

1 Introduction

One prominent application of Wireless Sensor Networks (WSN) is the detection of targets crossing a Field of Interest (*FoI*) [1]. As an example, in a physical intrusion detection system, sensors are deployed within the *FoI* to detect any intruders moving in restricted areas. In cases where the *FoI* is easily accessible, deploying the sensors in a deterministic manner provides worst case guarantees on the WSN performance that are not achievable by a stochastic sensor deployment. However, even in deterministic deployment scenarios, target detection can only be achieved probabilistically given random target trajectories, unless the entire boundary of the *FoI* is covered.

The quality of target detection achieved by a WSN has been quantified based on different design objectives [2–8]. A fundamental performance metric of the target detection capability of a WSN is the probability of detecting a target by at least one sensor [3]. This metric provides a worst case probabilistic guarantee on the Boolean determination of the existence of a target. However, in many applications, determining the existence of a target is not sufficient to trigger an appropriate action. Instead, additional information may be required such as the size, location and direction of the target. In such a case, the target has to be

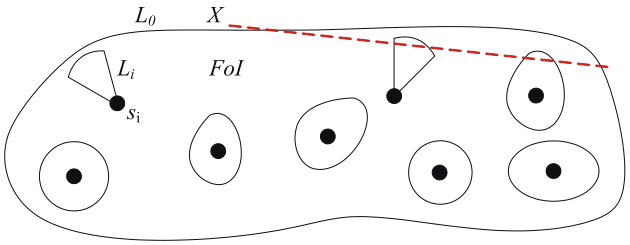

Fig. 1 A WSN monitoring an *FoI* with perimeter length L_0. The target X is crossing the *FoI* is detected if its trajectory intersects the sensing region of any sensor s_i. The deployed sensors have heterogeneous sensing regions of different shape and size

detected by a number of sensors larger than one, in order to achieve robust detection and characterization of the target. For such applications, the probability of collaboratively detecting a target by k sensors is the relevant target detection performance metric. Collaborative detection can reduce the target detection false alarm rate, as more sensors need to concur on the existence of the target, and provides additional information such as precise target location, direction or velocity. As an example, distance measurements from at least three (four) sensors to the target can be used to estimate the position of the target on the plane (space) using multilateration or maximum likelihood estimation [9, 10].

In this article, we analyze the following target detection problem. Given a *FoI* and N sensors, *determine the WSN constellation that yields the maximum target detection probability*. The target detection probability is a function of the number of sensors deployed, the relative positions of the sensors (WSN constellation), as well as the modality used to detect targets. The sensing modality defines the size and shape of the sensing region of the sensors deployed to detect the target. Oftentimes, a multi-modal approach is preferred in order to increase the robustness of the target detection process, by deploying sensors of different sensing modalities, such as acoustic, seismic, optical, or infrared [11]. As an example, in an intrusion detection application CCD sensors can be used to visually detect a sensor during the day, while detection can be assisted by acousting sensors during the night. In such a case, the sensor devices deployed have heterogeneous sensing regions, a reality significantly different from the unit disk model assumed in previous works [2–4, 7], or the assumption of identical sensing regions [2–8]. In Fig. 1, we show a WSN with heterogeneous sensing capabilities detecting a target X crossing the *FoI*.

1.1 Our contributions

In this article we make the following contributions. We map the target detection problem to a line-set intersection problem. Using tools from Integral Geometry we derive analytical formulas that characterize the target detection probability when sensors are deterministically deployed. Our derivations characterize the target detection capability both on the plane and in space. We consider two quantifiable metrics, that is, the worst case detection probability by at least one sensor, and the collaborative detection by k sensors. Compared to previous works [2–8, 12], we evaluate the target detection capability for WSN with devices of heterogeneous sensing capabilities. Based on our mapping, we show the number of terms in the analytical expression of the probability of target detection grows exponentially with the network size. We therefore provide appropriate lower and upper bounds. We show that as the pairwise distance among the sensors increases, the lower bound asymptotically approaches the upper bound and, hence, the probability of target detection is maximized. We also show that maximizing the lower bound of the probability of target detection is analogous to minimizing the average symbol error probability in two-dimensional and three-dimensional digital modulation schemes over an Additive White Gaussian Noise (AWGN) channel. In turn, the latter problems can be addressed by considering the circle packing problem on the plane and the sphere packing problem in the space. Inspired by this analogy, we examine the performance of known signal constellations on the target detection problem.

1.2 Paper organization

The rest of the paper is organized as follows. In Sect. 2, we present related work. In Sect. 3, we state our model assumptions and map the target detection problem to a line-set intersection problem. In Sect. 4, we derive exact analytical formulas for the target detection probability by at least one sensor on the plane, and describe the analogy of target detection to the two-dimensional digital modulation schemes over an AWGN channel. We further analyze the problem of collaborative target detection on the plane. In Sect 5, we analyze the problem of target detection in space, and present the analogy of target detection to three-dimensional modulation schemes over an AWGN channel. In Sect. 6, we present our performance evaluation and in Sect. 7, we present our conclusions.

2 Related work

The problem of detecting mobile targets in WSN has been a topic of extensive study under different metrics and assumptions [2–8, 12–15]. In [7], the authors investigate the trade off between the target detection quality and power

conservation. They assume that nodes are randomly deployed within a planar *FoI*, and have sensing regions that follow the unit disk model. Given a target X moving on a straight line, they derive the mean time until X is first detected. They also provide sleeping pattern algorithms that lead to power conservation, while guaranteeing a minimum response time to detecting a target crossing the *FoI*.

In [3], the authors provide analytic formulas for the mean delay until a target is detected, when targets move on a straight line at a constant speed. The authors consider a system model where N sensors are randomly distributed within an *FoI*, with each sensor having identical sensing regions that follow the unit disk model. In their derivations, they also take into account the sleeping pattern of the sensors.

In [8], the authors propose a collaborative detection model, where sensors collectively arrive at a consensus about the presence of a target. While the problem addressed in [8] is the coverage of the *FoI*, the problem formulation can be indirectly used to also evaluate the target detection probability. It is assumed that the detection capability of each sensor decays as a function of distance and hence, the sensing region of each sensor follows the unit disk model. In terms of performance metrics, the authors consider the minimum exposure path, that is, the path for which the target is least exposed to detection, and the maximum exposure path, that is, the path for which the target is most exposed to detection.

In [5], the authors consider the same collaborative detection model as in [8], with sensors collectively determining the presence of a target. Sensors are assumed to be randomly deployed within the *FoI* and the sensing capability of each sensor is assumed to decay with distance, with all sensors having identical sensing regions. They formulate the target detection problem as an unauthorized traversal problem and propose deployment strategies for minimizing the cost of the network that achieves the desired target detection probability. The authors proposed a deployment strategy where only part of the available sensors are randomly deployed. If the partial deployment satisfies the performance metric, no more sensors are deployed. Otherwise the process is repeated until the performance threshold is met.

In [12], the authors address the problem of optimum k-coverage of the boundary of an *FoI*. Covering the boundary of an *FoI* guarantees that any intruder will be detected with certainty. They assume that all sensors have identical sensing regions following the unit disk model as well. While target detection is guaranteed when the boundary of the *FoI* is covered, placement at the perimeter of the *FoI* does not yield the maximum target detection probability, when the boundary is not covered.

In [6], the authors address the problem of determining the delay until a target (intruder) is first detected. They consider the detection problem under the additional constraint that any sensor detecting the target must have a connected path to the sink. They assume that targets move in a straight line, and all sensors have identical sensing regions conforming to the unit disk model.

In [13], we considered the problem of target detection on the plane, under a heterogeneous sensing model. We assumed that the sensors are randomly deployed within the *FoI* and the sensing region of each sensor can have any arbitrary shape. Using tools from integral geometry, we derived analytic formulas for the probability of target detection by at least k sensors on the plane. We also evaluated the mean free time until the target is first detected by a sensor. However, we did not consider the problem of collaborative target detection, and the problem of target detection in space. In [14], we considered the problem of deterministic sensor deployment of heterogeneous sensor networks for maximizing the target detection probability by at least one sensor. Compared to [14], in our present work we additionally consider the case where the WSN is deployed in the space, and we also analyze the case of collaborative target detection where k sensors concurrently detect the presence of a target.

A relevant problem to target detection is the problem of target tracking. Once the target X has been detected, the WSN is used to track the motion of X within the *FoI*. Several methods for tracking moving targets with WSNs have been proposed in the literature [2, 7, 15, 16]. We do not address the problem of target tracking in this article.

3 Network model assumptions and problem mapping

3.1 Network model assumptions

Sensor deployment and field of interest, *FoI*. We assume that N sensors are available for placement within an *FoI*, $\mathcal{A}_0$. We consider two possible cases for the *FoI*:

(a) *Planar FoI*—In the planar case, we assume that the $\mathcal{A}_0$ is a connected and bounded set of arbitrary shape. If $\mathcal{A}_0$ is convex, its perimeter L_0 is bounded and assumed to be known. If $\mathcal{A}_0$ is not convex, we assume that the bounded perimeter L_0^h of the convex hull of $\mathcal{A}_0$ is known.

(b) *Three-dimensional FoI*—In the three-dimensional case, we assume that the *FoI*, $\mathcal{A}_0$, is a three-dimensional bounded and connected set of arbitrary shape. If $\mathcal{A}_0$ is convex, its surface area F_0 is bounded and assumed to be known. Otherwise, we assume that the bounded surface area F_0^h of the convex hull of $\mathcal{A}_0$ is known.

Target model: We assume that mobile targets move on straight line trajectories, and all possible trajectories

crossing the *FoI* appear with equal probability. Several targets such as signals (infrared, acoustic, electromagnetic) can be modeled as targets with straight line trajectories. Furthermore, for targets that do not follow the straight line assumption, a straight line approximation of the target trajectory provides the worst case analysis for the probability of detection. This is due to the fact that straight lines minimize the length of the path for which a target remains exposed for detection. Hence, given an entry and exit point, the probability of detecting a target moving on a straight line yields the worst case probability compared to the detection of any other possible trajectory. Straight line motion models have also been assumed in previous works addressing the target detection problem [3, 6, 7, 13, 14].

Sensing model: We assume that each sensor s_i, $i = 1,\ldots, N$ has a sensing region $\mathcal{A}_i$. We consider two possible cases for sensors deployed on the plane and in space:

(a) *Sensors with planar sensing region* $\mathcal{A}_i$—In the planar case, we assume that the $\mathcal{A}_i$ is a connected and bounded set of arbitrary shape. If $\mathcal{A}_i$ is convex, its perimeter L_i is bounded and assumed to be known. Otherwise, the bounded perimeter L_i^h of the convex hull of $\mathcal{A}_i$ is assumed known.

(b) *Sensors with three-dimensional sensing region* $\mathcal{A}_i$—In the three-dimensional case, we assume that $\mathcal{A}_i$ is a three-dimensional bounded and connected set of arbitrary shape. If $\mathcal{A}_i$ is convex, its surface area F_i is bounded and assumed to be known. If $\mathcal{A}_i$ is not convex, we assume that the bounded surface area F_i^h of the convex hull of $\mathcal{A}_i$ is known.

For detecting a mobile target X we assume the Boolean detection model, where a target X is detected by a sensor s_i if the trajectory of X crosses the sensing region of s_i. The Boolean detection model has also been assumed in [3, 12–14]. We further assume that sensors obtain correlated detection observations when their sensing regions overlap. The observation correlation ρ is a function of the pairwise distance $d_{i,j}$ between the sensors with overlapping sensing regions [17]. While it is more realistic to consider different correlation coefficients for sensors with different modalities, for simplicity we assume that all sensing modalities follow the same correlation model. The correlation between k sensors with overlapping sensing regions can be expressed as:

$$\rho = \begin{cases} \rho(d_{1,2}, d_{1,3}, \ldots, d_{k-1,k}), & \bigcap_{i=1}^{k} \mathcal{A}_i \neq \emptyset \\ 0, & \text{otherwise}, \end{cases} \quad (1)$$

where the correlation function is limited to $\rho \in [0, 1]$ and is assumed to be monotonically decreasing with the pairwise distances $d_{i,j}$. The decrease of ρ can be assumed to be linear, polynomial or even exponential.

Target detection metrics: We consider the following metrics for quantifying the detection capability of a WSN.

(a) *Detection by at least one sensor:* This metric quantifies the probability that the target X is detected by at least one sensor, or equivalently, that the trajectory of the target intersects the sensing region of at least one sensor. We denote this probability as,

$$P_D = P[\text{Target is detected by at least one sensor}]. \quad (2)$$

(b) *Collaborative target detection by k sensors:* This metric quantifies the probability that the target X is *collaboratively* detected by k sensors. Collaborative target detection increases the fault tolerance of the WSN, since multiple sensors verify the presence of a target at a given region, by sampling that reason from different locations. Furthermore, collaborative detection can by used to accurately localize the target X. If three (four) sensors can measure their distance from the target X at the same time, X can be localized in the plane (space) using multilateration methods [9, 10]. We denote the probability of collaborative target detection by k sensors as,

$$C_D = P[\text{Target is detected by } k \text{ sensors}]. \quad (3)$$

3.2 Mapping the target detection problem to the line-set intersection problem

In this section, we present the mapping of the target detection problem to the line-set intersection problem. This problem formulation provides the necessary tools to derive analytic formulas for the probability of target detection. We consider the problem of target detection under both metrics P_D, C_D.

Target Detection Problem: *Given an FoI* $\mathcal{A}_0$ *and N sensors* s_i, $i = 1,\ldots,N$, *with sensor* s_i *having a sensing region* $\mathcal{A}_i$, *find the WSN constellation that maximizes the probability* P_D *of detecting a target X randomly crossing* $\mathcal{A}_0$. *Also find the WSN constellation that maximizes the probability* C_D *of collaboratively detecting a target X by k sensors.*

Let the *FoI* be mapped to a bounded and closed set S_0, defined as a collection of points on the plane or in space. Let also the sensing region of sensor s_i be mapped to a bounded and closed set S_i. Note that the physical characteristics of the sensors guarantee that the sensing region of each sensor is indeed a closed and bounded set (limited transmission power). Let also the trajectory of the target X be mapped to a straight line ℓ on the plane or in space. Then, the target detection problem is equivalent to the following line-set intersection problem, arising in Integral Geometry [18, 19].

Line-set Intersection Problem: *Given a bounded and closed set* S_0 *and N sets* S_i, $i = 1,\ldots, N$, *find the positions of* S_i *inside* S_0 *that maximize the probability* P_D *that a random line* ℓ *intersecting* S_0, *also intersects any of the N sets* S_i.

Also find the positions of S_i that maximize the probability C_D that a random line ℓ crosses the intersection of k sets.

Throughout the rest of the paper we will use $\mathcal{A}_i$ to denote both the sensing region of sensor s_i and the corresponding set S_i.

4 Deterministic sensor deployment on the plane

4.1 Sensor placement for maximizing P_D

In this section, we analyze the problem of deterministic sensor placement on the plane. We compute the target detection probability by at least one sensor P_D as a function of the number of sensors deployed, the relative distance among sensors, and the perimeter of the sensing regions of each sensor. First, we derive analytical formulas when only one sensor is deployed within the *FoI*. Then, we extend to the case where two sensors are deployed within the *FoI*, and show the placement of those sensors that maximize P_D. We then generalize for the case of N sensors, and derive relevant lower and upper bounds on P_D using the cases of one and two sensors as building blocks.

4.1.1 Probability of target detection—deployment of a single sensor

Let a single sensor $\mathcal{A}$ be deployed within the *FoI*, $\mathcal{A}_0$. Let also a target X move on a straight line trajectory $\ell(\xi, \theta)$, where ξ denotes the shortest distance of the line to the origin of a fixed coordinate system, and θ denotes the angle of the direction perpendicular to the line ℓ, with the x-axis of the coordinate system. In Fig. 2(a), we show the parametrization of the line ℓ with respect to ξ, θ.

Given the single sensor deployment, the probability P_D of detecting the target X crossing the *FoI* can be derived using a frequency count argument. The P_D can be computed as the quotient of the "number" of lines in the plane crossing $\mathcal{A}_0$, over the "number" of lines crossing both $\mathcal{A}_0, \mathcal{A}$. In Fig. 2(b), we show the "number" of lines crossing the sensing region $\mathcal{A}_0, \mathcal{A}$, and the "number" of lines crossing $\mathcal{A}$, for a fixed trajectory direction θ. Since the set of lines in the plane intersecting a set $\mathcal{A}$ is uncountable, we use a measure defined in Integral Geometry [18–20].

Definition 1 Measure of set of lines $m(\ell)$ on the plane: The measure $m(\ell)$ of a set of lines $\ell(\xi, \theta)$ on the plane, is defined as the integral over the line density $d\ell = d\xi \wedge d\theta, m(\ell) = \int d\xi \wedge d\theta$, where $\wedge$ denotes the exterior product used in exterior calculus.

Definition 1 satisfies the measure criterion for the problem at hand. We want the measure of a set of line $m(\ell)$ to be invariant under the group of rigid motions, that is, rotation, translation and reflection. Intuitively, the measure of the set of lines $m(\ell)$ crossing a set $\mathcal{A}$ shall not change if $\mathcal{A}$ is moved anywhere within the plane, and arbitrarily rotated about any point in the plane. These conditions are satisfied by the form of $m(\ell)$ in Definition 1 and, hence, $m(\ell)$ can serve as a measure for our problem. In the case where $\mathcal{A}$ is convex, the measure of the set of lines that intersect $\mathcal{A}$ is equal to:

$$m(\ell : \ell \bigcap \mathcal{A} \neq \emptyset) \overset{\text{(i)}}{=} \int_{\ell \bigcap \mathcal{A} \neq \emptyset} d\xi \wedge d\theta \overset{\text{(ii)}}{=} \int_0^{2\pi} \xi d\theta = L, \qquad (4)$$

where L is the perimeter of $\mathcal{A}$. In Step (i), we integrate the line density over all lines on the plane that intersect $\mathcal{A}$, to obtain the measure of lines intersecting $\mathcal{A}$, per our Definition 1. In Step (ii), we keep ξ constant for a small change in the angle θ, and integrate over all possible θ. Interested reader is referred to [18–20] for a more elaborate proof of (4).

In the case where $\mathcal{A}$ is non-convex, any line intersecting the convex hull of $\mathcal{A}$, also intersects $\mathcal{A}$. Hence, $m(\ell)$ is

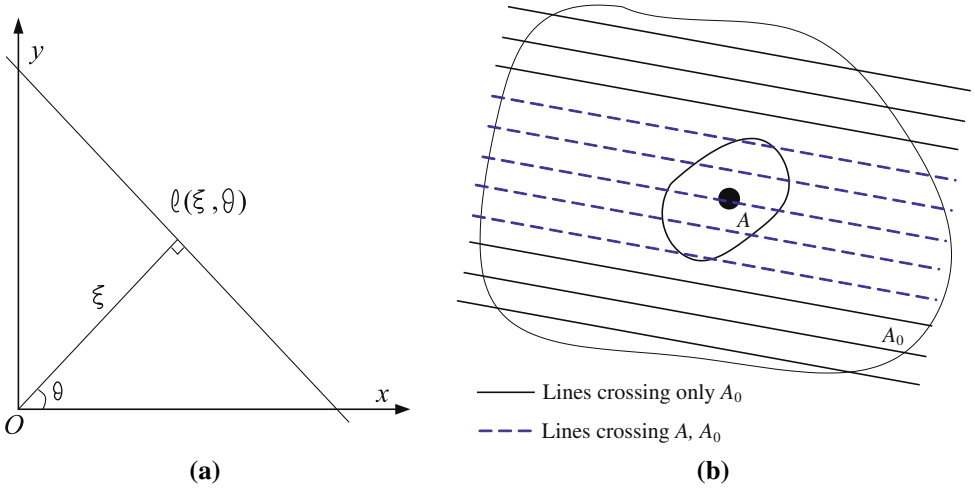

Fig. 2 (**a**) A line $\ell(\xi, \theta)$ on the plane, parameterized by the distance ξ of the line from the origin of the coordinate system, and the angle θ of the line perpendicular to ℓ, with respect to the x-axis. (**b**) The target detection probability P_D as the quotient of the "number" of lines crossing with the *FoI* $\mathcal{A}_0$, over the "number" of lines crossing the sensing region of s $\mathcal{A}$, for a fixed target trajectory θ. The solid lines denote the line that only cross $\mathcal{A}_0$, while the dashed lines denote the lines that cross both $\mathcal{A}_0, \mathcal{A}$, for a fixed target trajectory θ

equal to the perimeter L^h of the convex hull of $\mathcal{A}$. In the rest of the paper we assume that the sensing regions are of convex shape with perimeter L. In the case of non-convex shapes the perimeter L of a sensing region $\mathcal{A}$ can be substituted with the perimeter L^h of the convex hull of $\mathcal{A}$. Once we have defined a measure for the set of lines intersecting a set $\mathcal{A}$, the probability of target detection by a single sensor, is given by the following theorem.

Theorem 1 *The probability that a target X is detected by a sensor s with sensing region $\mathcal{A}$ of perimeter L, deployed within a planar FoI $\mathcal{A}_0$ of perimeter L_0 is given by $P_D = \frac{L}{L_0}$, assuming that $\mathcal{A} \subseteq \mathcal{A}_0$.*

Proof The proof follows by noting that the probability of detecting a target is equal to the quotient of the measure of the set of lines intersecting both sets $\mathcal{A}_0, \mathcal{A}$, over the measure of the set of lines intersecting $\mathcal{A}_0$.

$$P_D = \frac{m(\ell : \ell \bigcap \mathcal{A} \bigcap \mathcal{A}_0 \neq \emptyset)}{m(\ell : \ell \bigcap \mathcal{A}_0 \neq \emptyset)} \overset{\text{(i)}}{=} \frac{m(\ell : \ell \bigcap \mathcal{A} \neq \emptyset)}{m(\ell : \ell \bigcap \mathcal{A}_0 \neq \emptyset)} \overset{\text{(ii)}}{=} \frac{L}{L_0}. \tag{5}$$

Step (i) is due to the fact that any line intersecting $\mathcal{A}$, also intersects $\mathcal{A}_0 (\mathcal{A} \subseteq \mathcal{A}_0)$. Hence, the measure of the set of lines intersecting $\mathcal{A} \bigcap \mathcal{A}_0$ is equal to the measure of the set of lines intersecting $\mathcal{A}$. Step (ii) follows from (4). □

Note that P_D is independent of the shape of $\mathcal{A}, \mathcal{A}_0$, but only depends on the perimeter L of the sensing region and the *FoI*. Thus, sensors that have sensing regions of different shape but same perimeter, yield the same target detection probability. Also P_D has the same value, regardless of the position of $\mathcal{A}$ within $\mathcal{A}_0$, due to the fact that all possible trajectories (lines) of target X are considered equiprobable.

In the case where the condition $\mathcal{A} \subseteq \mathcal{A}_0$ does not hold true, Theorem 1 can still be used to compute P_D. The probability of target detection is given by (5), by substituting the perimeter L of $\mathcal{A}$ with the perimeter of $\mathcal{A} \bigcap \mathcal{A}_0$. Note that since our goal is deterministic sensor deployment it is not beneficial to place $\mathcal{A}$ partially inside $\mathcal{A}_0$ since the P_D is reduced.

4.1.2 Probability of target detection—deployment of two sensors

Let two sensors s_i, s_j be deployed anywhere within the *FoI*. The placement of the sensors that maximizes P_D is provided by the following theorem.

Theorem 2 *The target detection probability P_D by two sensors s_i, s_j is maximized when s_i, s_j are placed at the opposite ends of the diameter of the FoI, and is given by:*

$$P_D = \frac{L_i + L_j - m_2(d_{i,j})}{L_0}, \tag{6}$$

with

$$m_2(d_{i,j}) = \begin{cases} L_i + L_j - L_{out}(d_{i,j}), & \mathcal{A}_i \bigcap \mathcal{A}_j \neq \emptyset, \\ L_{in}(d_{i,j}) - L_{out}(d_{i,j}), & \mathcal{A}_i \bigcap \mathcal{A}_j = \emptyset, \end{cases} \tag{7}$$

where $d_{i,j}$ denotes the pairwise distance between s_i, s_j; $m_2(d_{i,j})$ denotes the measure of the set of lines intersecting both $\mathcal{A}_i, \mathcal{A}_j$; $L_{in}(d_{i,j})$ denotes the length of the inner string wrapped around $\mathcal{A}_i, \mathcal{A}_j$ as shown in Fig. 3(b); and $L_{out}(d_{i,j})$ denotes the length of the outer string wrapped around $\mathcal{A}_i, \mathcal{A}_j$ as shown in Fig. 3(a), (b).

Proof For the case of two sensors s_i, s_j, a target X is detected if its trajectory crosses the sensing region of either s_i or s_j. The P_D is expressed as the probability that a random line intersects any of the two sets $\mathcal{A}_i, \mathcal{A}_j$ placed within the *FoI*.

$$\begin{aligned} P_D &= P(\ell \cap \mathcal{A}_i) + P(\ell \cap \mathcal{A}_j) - P(\ell \cap \mathcal{A}_i \cap \mathcal{A}_j) \\ &\overset{(i)}{=} \frac{L_i + L_j - m_2(d_{i,j})}{L_0}. \end{aligned} \tag{8}$$

In Step (i), $P(\ell \cap \mathcal{A}_i), P(\ell \cap \mathcal{A}_j)$ are computed using Theorem 1, and are independent of the positions of the two sets $\mathcal{A}_i \mathcal{A}_j$. However, the measure $m_2(d_{i,j})$ of the set of lines intersecting both $\mathcal{A}_i \mathcal{A}_j$, is a function of the relative distance $d_{i,j}$ between $\mathcal{A}_i \mathcal{A}_j$, and is computed based on the following two cases.

Case I—$\mathcal{A}_i \cap \mathcal{A}_j \neq \emptyset$: When $\mathcal{A}_i$, $\mathcal{A}_j$ overlap as shown in Fig. 3(a), $\mathcal{A}_c = \mathcal{A}_i \cup \mathcal{A}_j$, is a connected and bounded set,

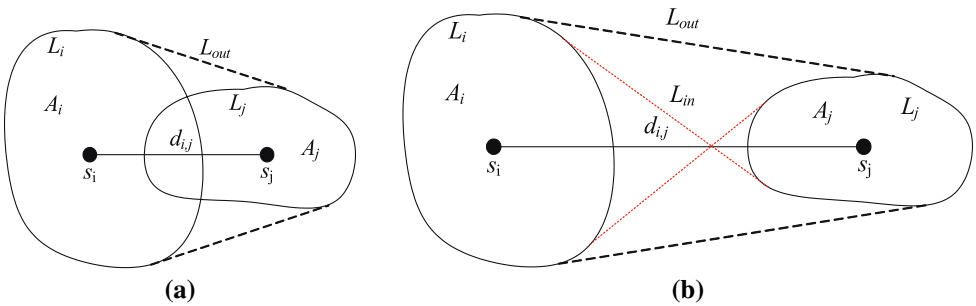

Fig. 3 The measure $m_2(d_{i,j})$ of the set of lines intersecting any of the two sensors is equal to (**a**) $L_{out}(d_{i,j})$ when $\mathcal{A}_i \cap \mathcal{A}_j \neq \emptyset$, (**b**) $L_i + L_j - (L_{in}(d_{i,j}) - L_{out}(d_{i,j}))$ when $\mathcal{A}_i \cap \mathcal{A}_j = \emptyset$

and the target X is detected if it crosses $\mathcal{A}_c$. According to (4), the measure of the set of lines intersecting $\mathcal{A}_c$ is equal to the perimeter of $\mathcal{A}_c$, when $\mathcal{A}_c$ is convex, or the perimeter of the convex hull of $\mathcal{A}_c$ when $\mathcal{A}_c$ is not convex. (when $\mathcal{A}_c$ is convex, $\mathcal{A}_c$ is the convex hull of itself by definition).

For two intersecting sets, the convex hull can be found by wrapping a string around the two sets, as shown in Fig. 3(a). Any line intersecting with the convex hull of $\mathcal{A}_c$, is guaranteed to intersect with at least one of $\mathcal{A}_i$, $\mathcal{A}_j$. Using Theorem 1, the target detection probability by two sensors with intersecting sensing regions is equal to:

$$P_D = \frac{L_i + L_j - m_2(d_{i,j})}{L_0} = \frac{L_{out}(d_{i,j})}{L_0}, \ \mathcal{A}_i \bigcap \mathcal{A}_j \neq \emptyset, \qquad (9)$$

where $L_{out}(d_{i,j})$ denotes the length of the perimeter of the convex hull of $\mathcal{A}_c$ (outer string in Fig. 3(a)). From (9), the measure of the set of lines intersecting both $\mathcal{A}_i$, $\mathcal{A}_j$ is, $m_2(d_{i,j}) = L_i + L_j - L_{out}(d_{i,j})$.

Case II—$\mathcal{A}_i \cap \mathcal{A}_j = \emptyset$: When the sensing regions $\mathcal{A}_i$, $\mathcal{A}_j$ do not overlap, as shown in Fig. 3(b), $\mathcal{A}_i$, $\mathcal{A}_j$ no longer form a connected and bounded set. Sylvester showed that the measure of all lines that intersect both $\mathcal{A}_i$, $\mathcal{A}_j$ is equal to $m_2(d_{i,j}) = L_{in}(d_{i,j}) - L_{out}(d_{i,j})$ [19]. Hence in the case of non-overlapping $\mathcal{A}_i, \mathcal{A}_j$, P_D is equal to:

$$P_D = \frac{L_i + L_j - m_2(d_{i,j})}{L_0} = \frac{L_i + L_j - (L_{in}(d_{i,j}) - L_{out}(d_{i,j}))}{L_0}. \qquad (10)$$

Corollary 1 *The measure $m_2(d_{i,j})$ of the set of lines intersecting two sets is a monotonically decreasing function of the pairwise distance $d_{i,j}$.*

Proof The proof is provided in the Appendix. □

Based on the monotonic behavior of $m_2(d_{i,j})$, the probability P_D increases as the distance $d_{i,j}$ increases. Given an *FoI* that is sufficiently large as it is implied by the assumption $\mathcal{A}_0 >> \mathcal{A}_i, \forall i$, the fraction of the set of lines crossing both sensors over the set of line crossing the *FoI* asymptotically approaches a negligible value with the increase of $d_{i,j}$.

In Fig. 4(a), we show the asymptotic behavior of P_D, as a function of $d_{i,j}$, for the case of two sensors. We observe that as $d_{i,j}$ increases, P_D tends to the asymptotic value of $\frac{L_i+L_j}{L_0}$. In Fig. 4(b), we show the monotonically decreasing behavior of the probability that a target crosses both sensing regions.

Given the boundary of the *FoI*, P_D is maximized when $d_{i,j}$ is maximized, which occurs when $\mathcal{A}_i$, $\mathcal{A}_j$ are placed at the opposite ends of the diameter of the *FoI*. In Fig. 5, we show the optimal placement of two sensors in the diameter of an a circular *FoI* and an *FoI* of arbitrary shape.

In the general case where $\mathcal{A}_i$, $\mathcal{A}_j$, have an arbitrary shape, an analytic formula for L_{in}, L_{out} may not be obtainable. Instead, $L_{in}(d_{i,j})$,$L_{out}(d_{i,j})$ may be measured, given that $\mathcal{A}_i$, $\mathcal{A}_j$ are known. On the other hand, for specific shapes of $\mathcal{A}_i$, $\mathcal{A}_j$, the lengths L_{in}, L_{out} can be expressed as a function of the distance $d_{i,j}$ among the shapes. As an example, for two circles with radius r,

$$L_{out} = 2(\pi r + d_{i,j}),$$
$$L_{in} = 2\pi r + 2d_{i,j}\sqrt{1 - \left(\frac{2r}{d_{i,j}}\right)^2} + 4\sin^{-1}\left(\frac{2r}{d_{i,j}}\right), \qquad (11)$$

when $d_{i,j} \geq 2r$. In the next section we utilize the P_D formula for the case of two sensors, in order to derive a lower bound on P_D for the case of N sensors.

4.1.3 *Probability of target detection—generalization to the deployment of* N *sensors*

When N sensors can be placed within the *FoI*, the probability of detecting a moving target is expressed based on the inclusion-exclusion principle for unions of sets [19, 21].

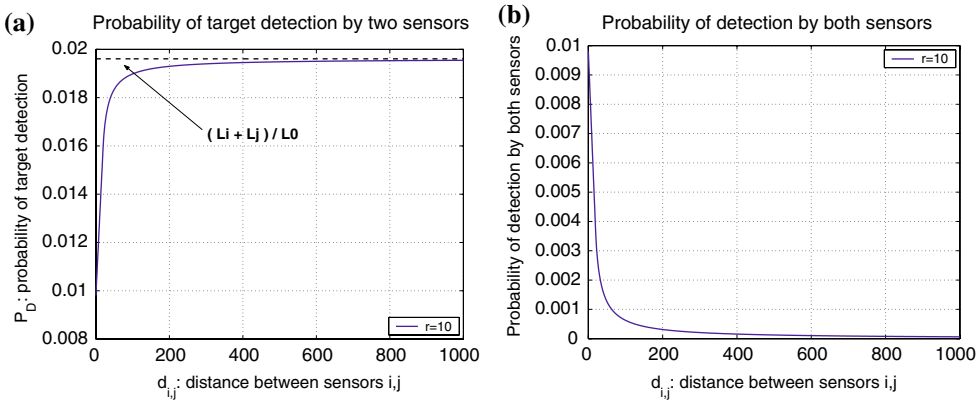

Fig. 4 The target detection probability P_D achieved by two sensors, as a function of the pairwise distance $d_{i,j}$ between the sensors, when each sensor has a circular sensing region of radius 10 m. P_D is a monotonically increasing function of $d_{i,j}$ that asymptotically approaches $\frac{L_1+L_2}{L_0}$. (b) The probability that a target is detected by *both* sensors is a monotonically decreasing function of the pairwise distance $d_{i,j}$, asymptotically approaching zero

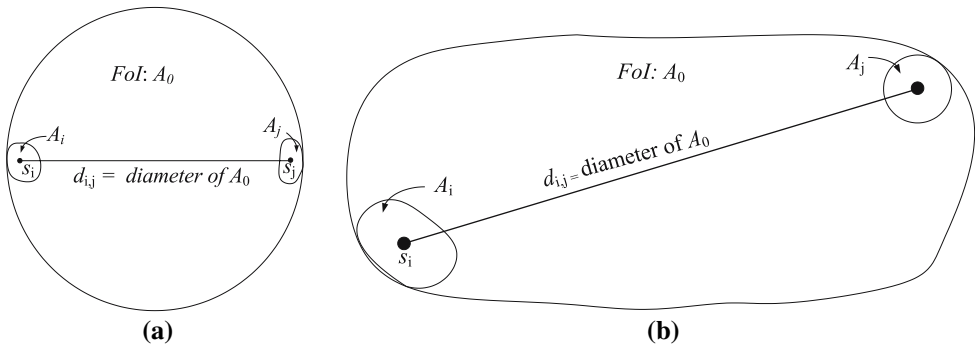

Fig. 5 Optimal placement of two sensors that maximizes the target detection probability P_D. Sensors s_i, s_j are placed at the opposite ends of the diameter of the *FoI*. (**a**) A symmetric *FoI*. (**b**) A non-symmetric *FoI*. The diameter is defined as the longest distance among two points within the *FoI*

Theorem 3 *Let a target X cross an FoI of perimeter L_0. Let N sensors be placed within the FoI at any desired position. The probability of detection P_D is given by*:

$$P_D = \sum_{i=1}^{N} P(\ell \cap \mathcal{A}_i \neq \emptyset) - \sum_{i,j,i<j} P(\ell \cap \mathcal{A}_i \cap \mathcal{A}_j \neq \emptyset) + \cdots + (-1)^{N+1} P(\ell \cap \mathcal{A}_1 \cap \cdots \cap \mathcal{A}_N \neq \emptyset). \quad (12)$$

Proof Given that N sensors are placed within the *FoI*, the probability that target X is detected is equivalent to the probability that X crosses the sensing region of at least one sensor. Expressing this statement in terms of probability events, we have

$$P_D = P(\ell \cap \mathcal{A}_1 \cup \mathcal{A}_2 \cup \cdots \cup \mathcal{A}_N). \quad (13)$$

By applying the inclusion-exclusion principle [21], P_D is expressed using the sum of conjunctive probabilities of a line intersecting specific arrangements of sets.

$$\begin{aligned} P_D &= P(\ell \cap \mathcal{A}_1 \neq \emptyset) + P(\ell \cap \mathcal{A}_2 \neq \emptyset) \\ &\quad + \cdots + P(\ell \cap \mathcal{A}_N \neq \emptyset) - P(\ell \cap \mathcal{A}_1 \cap \mathcal{A}_2 \neq \emptyset) \\ &\quad - P(\ell \cap \mathcal{A}_1 \cap \mathcal{A}_N \neq \emptyset) \cdots + (-1)^{N+1} \\ &\quad \times P(\ell \cap \mathcal{A}_1 \cap \mathcal{A}_2 \cdots \cap \mathcal{A}_N \neq \emptyset) \\ &= \sum_{i=1}^{N} P(\ell \cap \mathcal{A}_i \neq \emptyset) - \sum_{i,j,i<j} P(\ell \cap \mathcal{A}_i \cap \mathcal{A}_j \neq \emptyset) \\ &\quad + \cdots + (-1)^{N+1} P(\ell \cap \mathcal{A}_1 \cap \mathcal{A}_2 \cdots \cap \mathcal{A}_N \neq \emptyset). \end{aligned}$$

□

While Theorem 3 expresses the exact analytic formula for P_D, the number of terms in (12) is $(2^N - 1)$. Furthermore, for arbitrary set arrangements, analytic expressions of the probability of a line intersecting exactly k sets are not known, except for small values of k [19]. Hence, we consider the following lower and upper bounds for finite unions.

Corollary 2 *The probability of target detection P_D is bounded by:*

$$\sum_{i=1}^{N} P(\ell \cap \mathcal{A}_i \neq \emptyset) - \sum_{i,j,i<j} P(\ell \cap \mathcal{A}_i \cap \mathcal{A}_j \neq \emptyset) \leq P_D \leq \sum_{i=1}^{N} P(\ell \cap \mathcal{A}_i \neq \emptyset). \quad (14)$$

Proof This is a special case of the Bonferroni inequalities [21]. □

Both the lower and upper bound in (14), can be evaluated using the results of Theorems 1, 2:

$$\frac{1}{L_0}\left(\sum_{i=1}^{N} L_i - \sum_{i,j,i<j} m_2(d_{i,j})\right) \leq P_D < \frac{1}{L_0}\sum_{i=1}^{N} L_i. \quad (15)$$

The lower bound in (15) is exact for sensor constellations where no lines intersect more than two sensing regions. However, we note that P_D can never achieve the upper bound for $N > 1$ since there will always be a non-zero "number" of lines crossing two sensing regions. The lower bound approaches the upper bound as the pairwise distances $d_{i,j}$ among each pair of sensors increase. This is a consequence of the asymptotic behavior of P_D for $N = 2$, as we showed in Sect. 4.1.2. Hence, by increasing the pairwise distance $d_{i,j}$ among each pair of sensors, the lower bound of P_D tends to the upper bound and, hence, P_D attains its maximum value. Assuming that L_0 is sufficiently large so that $\frac{m_2(d_{i,j})}{L_0} \approx 0$, when $d_{i,j}$ is large,

$$\frac{1}{L_0}\left(\sum_{i=1}^{N} L_i - \sum_{i,j,i<j} m_2(d_{i,j})\right) = \frac{1}{L_0}\sum_{i=1}^{N} L_i - \frac{1}{L_0}\sum_{i,j,i<j} m_2(d_{i,j}) \approx \frac{1}{L_0}\sum_{i=1}^{N} L_i. \quad (16)$$

In Fig. 6(a), we show the values for the lower and upper bound of P_D as a function of the pairwise distance among sensors. The sensing regions of the sensors are assumed disks with radius $r = 10$ m while the *FoI* is assumed to be a disk of radius $R = 1{,}000$ m. The x-axis is normalized to the radius of the sensing regions of the sensors. We observe that for small values of the pairwise distance, the lower

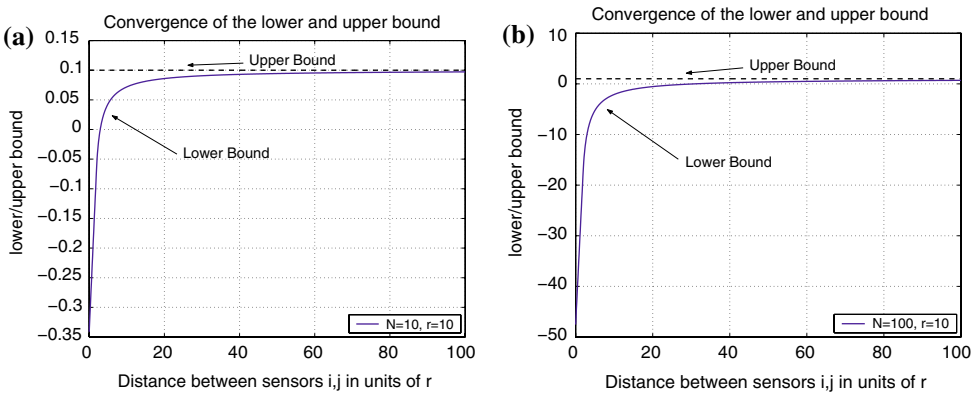

Fig. 6 Convergence of the lower bound of P_D to the upper bound of P_D with the increase of the pairwise distance $d_{i,j}$ for a WSN of (**a**) 10 nodes, (**b**) 100 nodes. The x-axis denotes the pairwise distance normalized in units of the sensing range of the sensors r

bound does not reflect the actual value of P_D. In fact, the lower bound has negative value since the higher order terms that are ignored (probabilities that lines cross three or more sensing regions) are significant. However, when the pairwise distances become sufficiently large, ($d_{i,j} \geq 20r$), the lower bound approaches the upper bound and P_D tends asymptotically to the upper bound. Similarly, in Fig. 6(b), we show the convergence of the lower and upper bound for $N = 100$ sensors. For larger N the lower and upper bound convergence is slower compared to the case of $N = 10$.

4.1.4 Analogy of target detection to two-dimensional digital modulation schemes

Maximizing the lower bound in (15), provides a worst case probabilistic guarantee on target detection. The first sum of the lower bound in (15) is independent of the sensors' positions. On the other hand, the sum $\sum_{i,i<j} m_2(d_{i,j})$ is a function of the pairwise distance $d_{i,j}$, among the sensors. In Sect. 4.1.2, we showed that $m_2(d_{i,j})$ is a positive monotonically decreasing function of $d_{i,j}$. Hence, increasing $d_{i,j}$ also increases the lower bound in (15). In fact, for sensor constellations where no lines intersect more than two sets, the lower bound is exact and hence, increasing the lower bound also increases P_D.

The problem of finding the sensor constellation that maximizes the lower bound in (15) is analogous to the problem of finding a two-dimensional signal constellation that minimizes the average probability of symbol error P_{SE}, over an AWGN channel. Assuming that all symbols are equiprobable, P_{SE} is expressed as a function of the pairwise error probability $P(b_i \rightarrow b_j)$ between two symbols b_i, b_j. $P(b_i \rightarrow b_j)$ is a monotonically decreasing function of $d_{i,j}$ between the two symbols [22]. For a constellation with N equiprobable symbols, P_{SE} is upper bounded by,

$$P_{SE} \leq \frac{1}{N} \sum_{i,i<j} P(b_i \rightarrow b_j) = \frac{1}{N} \sum_{i,i<j} \frac{1}{2} \mathrm{erfc}\left(\frac{d_{i,j}}{2\sqrt{N_0}}\right), \qquad (17)$$

where erfc denotes the error function, and $\frac{N_0}{2}$ denotes the power spectral density of the channel noise component. Both the problem of maximizing the lower bound in (15) and the analogous problem of minimizing P_{SE}, require the minimization of a multivariate function which is a summation of identical functions, monotonically decreasing with respect to each variable. This problem analogy is presented in Table 1.

In digital communications, the minimum pairwise distance among symbols is the dominant factor of symbol error, due to the exponential decrease of $P(b_i \rightarrow b_j)$ with $d_{i,j}$ [22]. Hence, good symbol constellations maximize the minimum pairwise distance among symbols. Due to the analogy presented in Table 1, we consider solutions that maximize the minimum pairwise distance for the target detection problem. The problem of maximizing the minimum pairwise distance among points in the plane, can be addressed using the following circle packing problem, as an intermediate step [23]. *Given N circles C_i, $i = 1,\ldots, N$, compute the maximum radius of the circles that would fit inside a given planar set $\mathcal{A}_0$.*

The circle packing problem, has known optimal solutions for small values of N, and certain shapes of *FoI*, such as circle, square, hexagonal or triangle, but no optimal solutions exist for large N [22, 24]. However, good signal constellations can be carved from lattices with high circle packing density [23]. In order to derive the sensor

Table 1 Analogy of the target detection probability to the symbol error probability

Mobile target detection	↔	Symbol error over AWGN
Number of sensors N	↔	Number of symbols N
Field of interest $\mathcal{A}_0$	↔	Maximum symbol energy
Sensor constellation	↔	Symbol constellation
Pairwise distance $d_{i,j}$ among sensors	↔	Pairwise distance $d_{i,j}$ among symbols
Monotonically decreasing function $m_2(d_{i,j})$	↔	Monotonically decreasing function $P(b_i \rightarrow b_j)$
Maximize the probability of target detection	↔	*Minimize the symbol error probability*

constellations that correspond to the solution of the circle packing problem we execute the following steps.

Step 1: Fit N circles $C_i(r)$, $i = 1,\ldots, N$ of equal radius r within the *FoI* so that the radius r is maximized (solution to the circle packing problem).
Step 2: For each circle $C_i(r)$ of the constellation, if C_i is on the perimeter of the *FoI*, place the sensor s_i within C_i so that the sensing region $\mathcal{A}_i$ is tangential to the perimeter of $\mathcal{A}_0$.
Step 3: If circle C_i is an inner circle (not tangent to the perimeter of the *FoI*), place the sensor s_i within C_i so that the sensing region $\mathcal{A}_i$ is centered to the center of C_i.

In Fig. 7(a), we show the optimum placement of circles that maximize the minimum pairwise distance among the circles, for a circular *FoI*, for $N = 2,\ldots, 9$. In Fig. 7(b), we show the optimum placement for the case of a square *FoI*. Note that the circles C_i defined from the circle packing problem do not correspond to the sensing regions $\mathcal{A}_i$ of the sensors. Instead they provide the region C_i where each sensor s_i should be placed. Assuming that $\mathcal{A}_i \ll C_i$ which holds true when $\mathcal{A}_i \ll \mathcal{A}_0$ and N is not sufficient to cover the *FoI*, the position of the sensors within C_i, is chosen so that the sensing regions have maximum pairwise distance. As an example, in Fig. 7(a) for the case of $N = 2$, the sensors are placed within C_1, C_2 so that the sensing regions have maximum $d_{i,j}$. For networks with heterogeneous sensing regions, sensors are placed within each C_i with the s_i with larger L_i be placed further apart.

4.2 Sensor placement for maximizing C_D

The goal of collaborative detection is to increase the reliability of the system in terms of the false positive and missed detection rates. A false positive can occur, for example, when the target is detected using acoustic sensors and the wave sound reaches the sensor via multipath. A missed detection can occur, for example, if the target is detected via ccd cameras, and an (temporary) obstacle obstructs the sensor view, hiding the presence of a target.

Using collaborative detection, the same space can be observed by multiple sensors from different location, thus spatially decorrelating the observations obtained from observing the same phenomenon. Furthermore, detecting the target via multiple sensors can enable the localization of the target via a localization algorithm [9, 10].

In this section, we analyze the probability of collaborative detection of a mobile target X crossing the *FoI*. We first consider the simple case where only two sensors are used to collaboratively detect a single target. Then we extend our analysis to the case where at k sensors collaboratively detect X. We finally analyze the case where N sensors are available for placement, when k-detection is required.

4.2.1 *Probability of collaborative detection—deployment of two sensors*

Let us consider the case where we want to maximize the probability of collaboratively detecting a target X using two sensors s_i, s_j. To achieve collaborative detection, the target X has to cross the intersection of the sensing regions of s_i,s_j, so that X is simultaneously detected by both s_i, s_j. Following the equivalence of the target detection problem to the line-set intersection problem as presented in Sect. 3.2, a target X is detected if its random trajectory crosses the intersection $\mathcal{A}_c$ of the sensing regions $\mathcal{A}_i, \mathcal{A}_j$, as shown in Fig. 8(a). Hence, in the case of collaborative detection, the sensing regions of the sensors s_i, s_j have to be placed in such a way that $\mathcal{A}_i, \mathcal{A}_j$, intersect.

Since $\mathcal{A}_i, \mathcal{A}_j$, are closed and bounded sets, their intersection $\mathcal{A}_c$ is also a closed and bounded set. Let P_c denote the probability that a random line crosses the intersection region $\mathcal{A}_c$. Based on Theorem 1, the probability P_c is a monotonically increasing function of the perimeter length L_c. Let the perimeter L_c of the intersection region $\mathcal{A}_c$ be expressed as a function of the pairwise distance $d_{i,j}$ between the sensors s_i,s_j. Based on Theorem 1, the probability P_c that a random line crosses the intersection region $\mathcal{A}_c$ is given by the quotient of L_c over the perimeter length of the *FoI*, L_0.

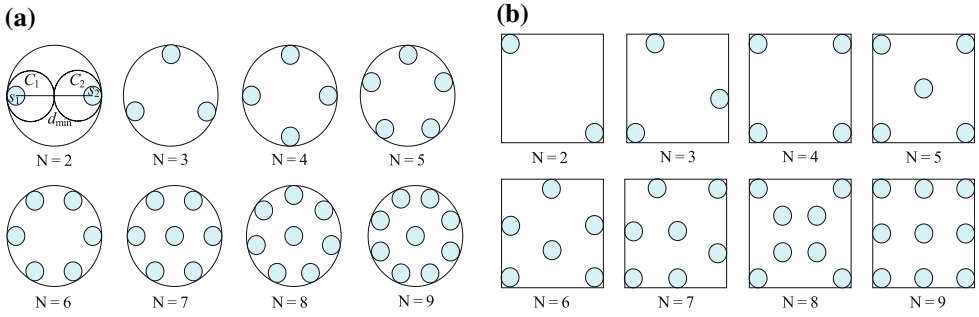

Fig. 7 The sensor constellations that maximize the minimum pairwise distance among sensors for, (**a**) a circular *FoI*, (**b**) a square *FoI*. The shaded circles denote the sensing region of each sensor

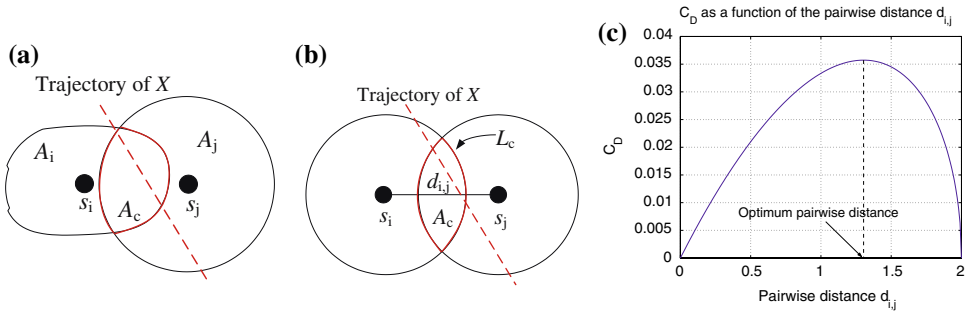

Fig. 8 (**a**) Collaborative detection of a target X by two sensors s_i, s_j with heterogeneous sensing regions. The trajectory of target X, denoted by the dashed line, has to cross the intersection of the sensing regions $\mathcal{A}_i, \mathcal{A}_j$ in order to be collaboratively detected. (**b**) Collaborative detection when the sensing regions of $\mathcal{A}_i, \mathcal{A}_j$ are circular with fixed radius r, with sensors s_i, s_j being at a distance $d_{i,j}$. (**c**) The collaborative detection probability C_D as a function of the pairwise distance $d_{i,j}$ normalized over the radius of the circular sensing regions of the sensors in Fig. 8(b). The C_D attains its maximum value at $d^*_{i,j} = 1.3r$

$$P_c(d_{i,j}) = \frac{L_c(d_{i,j})}{L_0}. \tag{18}$$

Note that the maximum perimeter L_c of the intersection region $\mathcal{A}_c$ is always upper bounded by the minimum of the perimeters L_i,L_j of the two sets $\mathcal{A}_i, \mathcal{A}_j$. Hence, the collaborative detection capability of the two sensors is always limited by the individual target detection capability of each sensor. Based on our sensing model as presented in Sect. 3.1, when two sensing regions overlap their observations are correlated, thus reducing the fidelity of target detection. By combining the probability of a random line crossing the intersection $\mathcal{A}_c$ and the correlation function $\rho(d_{i,j})$, we can compute the probability of collaborative detection C_D to be:

$$C_D(d_{i,j}) = \big(1 - \rho(d_{i,j})\big)\frac{L_c(d_{i,j})}{L_0}. \tag{19}$$

Optimizing C_D with respect to $d_{i,j}$, yields the relative distance of the two sensors that maximizes the probability of collaborative detection by two sensors. The optimum value $d^*_{i,j}$, that maximizes C_D in (19) is a function of the sensing regions of the two sensors s_i,s_j and the correlation model we consider. We now provide an example for the calculation of the optimal pairwise distance $d^*_{i,j}$.

Example on the calculation of the optimal sensor constellation of two sensors for maximizing the collaborative detection probability C_D–Let us assume for simplicity that the two sensors have identical sensing regions of circular shape of radius r, as shown in Fig. 8(b). Assume also that the correlation function $\rho(d_{i,j})$ decreases linearly as a function of the pairwise distance $d_{i,j}$. That is:

$$\rho(d_{i,j}) = \begin{cases} 1 - \frac{d_{ij}}{2r}, & \mathcal{A}_i \bigcap \mathcal{A}_j \neq \emptyset \\ 0, & \text{otherwise.} \end{cases} \tag{20}$$

The perimeter of the intersection region between two circles of the same radius is given by:

$$L_c(d_{i,j}) = 4r \arccos\left(\frac{d_{i,j}}{2r}\right). \tag{21}$$

Combining equations (20) and (21), yields the probability of collaborative target detection:

$$C_D(d_{i,j}) = \big(1 - \rho(d_{i,j})\big)\frac{L_c(d_{i,j})}{L_0} = \frac{2d_{i,j}\arccos\left(\frac{d_{i,j}}{2R}\right)}{L_0}. \tag{22}$$

Given that (22) has no analytic solution, we numerically solve for the optimal value of $d_{i,j}$ that maximizes C_D to be $d^*_{i,j} \approx 1.3r$. In Fig. 8(c) we show C_D as a function of $d_{i,j}$ normalized over the radius of the circular sensing regions r. For deriving C_D we considered circular sensing regions of radius $r = 10$ m and an *FoI* of perimeter 200π. Following a similar process, we can calculate the optimal distance $d^*_{i,j}$ for different correlation functions and for different shapes of the sensing regions $\mathcal{A}_i, \mathcal{A}_j$. Once the relative pairwise distance that maximizes C_D is obtained, placement of the sensor constellation anywhere within the *FoI*, yields the same target collaborative detection probability C_D due to the random target trajectory assumption.

4.2.2 *Probability of collaborative detection*—k *sensor deployment*

We now consider the case where we want to maximize the probability of collaboratively detecting a target X by $k > 2$ sensors. For collaborative detection by k sensors, the sensing regions of k sensors must overlap so that they can simultaneously detect the presence of a target X. A target X is detected, if its trajectory crosses the intersection of k sensing regions. As in the case of collaborative detection with two sensors, the probability of collaborative detection C_D is a function of the perimeter L_c of the intersection region $\mathcal{A}_c$ and the correlation among the observations of the sensors. Both the perimeter of the intersection region

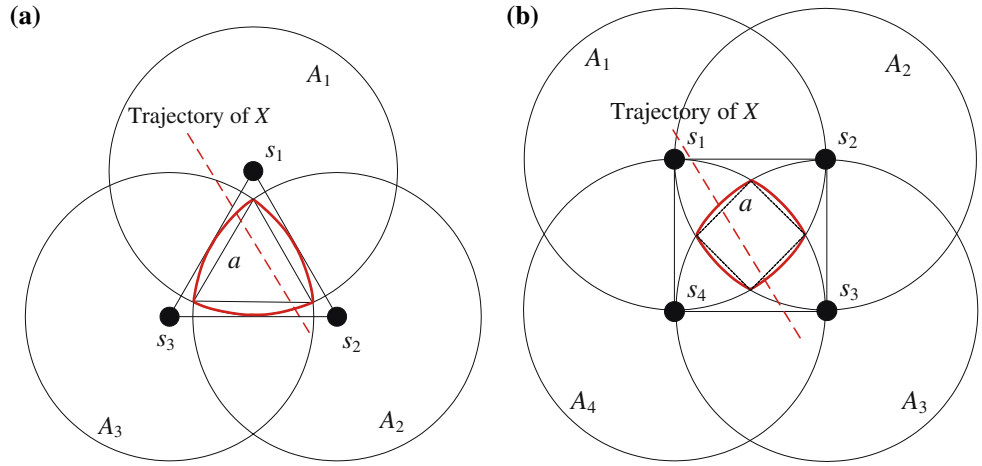

Fig. 9 (**a**) Collaborative detection of a target X by three sensors with circular sensing regions. The trajectory of target X, denoted by the dashed line, has to cross the intersection of the sensing regions in order for X to be collaboratively detected. The intersection region among the three sensing regions is a Reuleaux triangle of side α. (**b**) Collaborative detection of a target X by four sensors with circular sensing regions. The trajectory of target X, denoted by the dashed line, has to cross the intersection of the sensing regions in order for X to be collaboratively detected. The intersection region among the three sensing regions is a Reuleaux square of side α

and the correlation of the observations are a function of the pairwise distances $d_{i,j}$ among the k sensors that intersect. Let the sensing regions of sensors $s_1, s_2, \ldots, s_k$ intersect. The probability of collaborative detection C_D by the k-tuple of sensors is a multivariate function, of all the pairwise distances among the k intersecting sensors.

$$C_D = \big(1 - \rho(d_{1,2}, d_{1,3}, \ldots, d_{k-1,k})\big) \frac{L_c(d_{1,2}, d_{1,3}, \ldots, d_{k-1,k})}{L_0}. \tag{23}$$

The values of $d_{i,j}$ that maximize C_D depend on the specific forms of $\rho(d_{1,2}, d_{1,3}, \ldots, d_{k-1,k}), L_c(d_{1,2}, d_{1,3}, \ldots, d_{k-1,k})$. The simplest case for the multivariate correlation function $\rho(d_{1,2}, d_{1,3}, \ldots, d_{k-1,k})$ is to consider that it is symmetric over all variables $d_{i,j}$. For example in the linear case, the correlation function is given by the linear combination (or any weighted linear combination variant) of the pairwise correlation functions:

$$\rho(d_{1,2}, d_{1,3}, \ldots, d_{k-1,k}) = \begin{cases} 1 - \frac{d_{1,2}+d_{1,3}+\cdots+d_{k-1,k}}{2\binom{k}{2}r}, & \bigcap_{i=1}^{k} \mathcal{A}_i \neq \emptyset \\ 0, & \text{otherwise.} \end{cases} \tag{24}$$

The perimeter L_c of the intersection of the k sets, is a function of the pairwise distances among the sensors and the shapes of the sensing regions. In the simplest case where the sensors have circular sensing regions of the same radius r, and are placed at the vertices of a canonical k-vertex polygon, the intersecting region is a Reuleaux polygon of perimeter $L_c = 2\pi\alpha$, where α denotes the diameter or width of the polygon. Note that Reuleaux polygons have constant width, that is, their projection to a line of any direction is constant. In Fig. 9 we show the intersection of three and four circular sensing regions of same radius r.

When heterogeneous sensing regions are considered, it may not be feasible to obtain a closed analytical form expressing the perimeter of the intersection L_c. In such a case the optimization of C_D can be done numerically by considering a quantized version of all possible pairwise distances among the sensors under consideration. Note that for the majority of sensor applications, k is expected to be a small number, and hence, an exhaustive quantized search can be performed before deployment, to determine the k-sensor constellation that optimizes C_D.

4.2.3 *Probability of collaborative detection by* k *sensors—deployment of* N *Sensors*

Let $N > k$ sensors be available for placement within the *FoI*, and let k of them be sufficient for the collaborative detection of a target X. We want to find the sensor constellation that maximizes the collaborative target detection capability C_D of the WSN. For any sensor constellation, the probability of target detection is characterized by the number and relative distance of the distinct intersection regions $\mathcal{A}_{c_i}$ formed by the intersection of k sensors. Once the sensors are placed within the *FoI*, the collaborative detection probability C_D is given by Theorem 3. That is,

$$C_D = \sum_{i=1}^{N} P(\ell \cap \mathcal{A}_{c_i} \neq \emptyset) - \sum_{i,j,i<j} P(\ell \cap \mathcal{A}_{c_i} \cap \mathcal{A}_{c_j} \neq \emptyset) + \cdots + (-1)^{N+1} P(\ell \cap \mathcal{A}_{c_1} \cap \cdots \cap \mathcal{A}_{c_{N-1}} \neq \emptyset), \tag{25}$$

where the sensing regions $\mathcal{A}_i$ of Theorem 3 have now been substituted by the intersection regions $\mathcal{A}_{c_i}$ of k

sensing regions. As we showed in Sect. 4.1.3, the number of terms in (25) grows exponentially with the network size and not all terms can be analytically computed. Hence, we derived lower and upper bounds for the probability of target detection. Similarly, lower and upper bounds can be derived for the probability of collaborative detection C_D.

$$\sum_{i=1}^{N} P(\ell \cap \mathcal{A}_{c_i} \neq \emptyset) - \sum_{i,j,i<j} P(\ell \cap \mathcal{A}_{c_i} \cap \mathcal{A}_{c_j} \neq \emptyset) \leq C_D \leq \sum_{i=1}^{N} P(\ell \cap \mathcal{A}_{c_i} \neq \emptyset). \quad (26)$$

We now propose a heuristic sensor placement solution that generates the maximum number of non-overlapping intersection regions, with optimum sensor placement for the k-tuple of sensors. The process of finding the sensors' positions is equivalent to the process of generating a deterministic k-connected network where the degree of each node in the network is minimum.

4.3 A heuristic sensor placement algorithm for collaborative target detection

Let N sensors be available for placement within the *FoI* and let k of them be sufficient for the collaborative detection of a target X crossing the *FoI*. Let also the optimal placement of k sensors that maximizes the collaborative target detection probability as derived in Sect. 4.2.2 be known. For any k sensors placed within the *FoI* so that they collaboratively detect a target X, we can represent the sensor placement with a k-polygon Π_i where the k sensors are placed in the vertices of a k-polygon. The idea behind our heuristic is to generate the maximum number of k-polygons with the intersection regions formed by each k-tuple of sensors not to intersect.

Initially, we place k sensors to form the first k-polygon Π_1. We then find the minimum number of sensors that can be appended to the k-polygon Π_1 so that a new polygon Π_2 is created. If more than one choice is available, we create the k-polygon Π_2 that yields an intersection region $\mathcal{A}_{c_2}$ farthest away from the previously generated intersection region $\mathcal{A}_{c_2}$. This is preferred in order to minimize the probability that a random line can cross both intersecting regions. We repeat the process until all sensors are placed within the *FoI*. The sensor placement process can be outlined in the following steps:

Step 1: Place k sensors at the vertices of a k-polygon Π_1 so that the collaborative detection probability of the k-intersection region $\mathcal{A}_{c_1}$ is maximized (following the design principles of Sect. 4.2.2.)

Step 2: Select $(k - i)$ sensors to form another k-polygon Π_j, with variable i denoting the number of sensors reused from the previously formed polygons. The $(k - i)$ newly selected sensors combined with i previously placed sensors must generate a k-polygon with an intersecting region that does not overlap with any previously generated intersecting region.

Step 3: Add the selected $(k - i)$ sensors in such a way that the distance of $\mathcal{A}_{c_j}$ to all previously formed polygons is maximum, subject to the constraint that all sensors fall within the *FoI*.

Step 4: Repeat Steps 2–5, until all sensors have been placed within the *FoI*.

Let each sensor s_i be mapped to a network node V_i, and each side of a polygon be mapped to a network edge e_i. Then, our heuristic sensor placement process yields a $(k - 1)$ -connected network $G(V,E)$, with every border node having a degree $(k - 1)$ and every inner node having a degree k. Note that depending on the values of N, k there might be at most $(k - 3)$ remaining sensors that cannot form a k-polygon. For large values of N and small values of k as expected in realistic applications, the depredation in performance by not using the $(k - 3)$ sensors is negligible. We now provide examples of our heuristic placement algorithm for collaborative target detection.

4.3.1 *Examples of heuristic sensor placement for* k = *2,3*

Example 1 $k = 2$—Assume that two types of sensors are available for placement within the *FoI*, and we want to combine the two different sensing modalities to detect the presence of a target X. Based on Sect. 4.2.1, collaborative detection by two sensors is optimized when the sensors are placed at a distance d^* apart. This sensor constellation is the building block for the placement of the remaining sensors. Let sensor s_1, s_2 be placed so that they form an intersection region $\mathcal{A}_{c_1}$, when placed at an optimum distance d^*. By adding one more sensor s_3 at a distance d^* from either s_1 or s_2 we can generate one more intersection region $\mathcal{A}_{c_2}$. We place s_3 on the same line as the line formed by s_1, s_2, so as to maximize the separation of $\mathcal{A}_{c_2}$, from $\mathcal{A}_{c_1}$. By repeating the process, we place all N available sensors within the *FoI*.

In Fig. 10(a), we show the sensor placement of N sensors with two types of sensing regions, and the corresponding intersection regions $\mathcal{A}_{c_i}$. Our heuristic sensor placement algorithm forms a serial network with every border node having a degree of one, and every inner node having a degree of two. Note that the distance from any intersection region to any other intersection region is

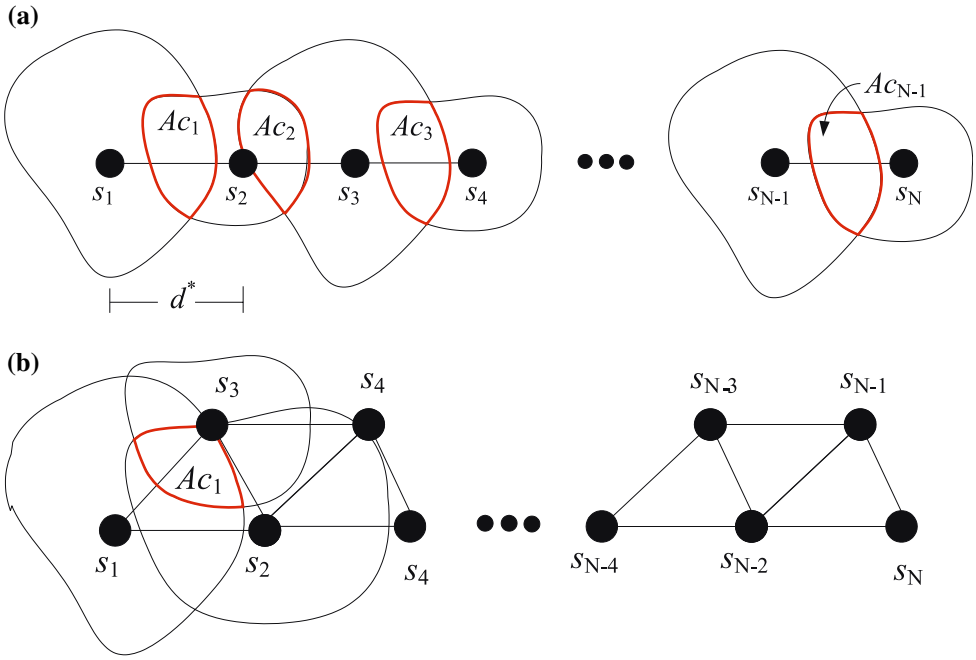

Fig. 10 (**a**) The sensor placement of N sensors with two types of sensing regions, and the corresponding intersection regions $\mathcal{A}_{c_i}$. Our heuristic sensor placement algorithm forms a serial network with every border node having a degree of one, and every inner node having a degree of two. (**b**) The sensor placement of N sensors with three types of sensing regions, and the corresponding intersection regions $\mathcal{A}_{c_i}$. Our heuristic sensor placement algorithm forms a 2-connected network

maximized as all network nodes are placed on a straight line. Also note that the number of intersecting regions formed by N sensors are equal to $(N-1)$. The collaborative probability of target detection for the sensor constellation depicted in Fig. 10(a) is lower bounded by:

$$C_D \geq \frac{1}{L_0}\left(\sum_{i=1}^{N} L_{c_i} - \sum_{i,j,i<j} m_2(d_{i,j})\right), \tag{27}$$

where L_{c_i} denotes the length of the perimeter of the intersection regions $\mathcal{A}_{c_i}$; $m_2(d_{i,j})$ denotes the measure of the set of lines crossing both intersection regions $\mathcal{A}_{c_i}, \mathcal{A}_{c_j}$; and $d_{i,j}$ is the pairwise distance among the sensors which is fixed to $d_{i,j} = |i-j|d^*$, with the distance d^* being the optimal distance among two sensors that maximizes C_D.

Example 2 $k = 3$—Let us now consider the case where we want to collaboratively detect a target X with three sensors. Again we compute the optimum pairwise distances among the three sensors that maximizes the collaborative target detection capability and form a triangle Π_1 that will serve as the k-component for our sensor placement. The minimum number of sensors to be added in order to form a new triangle Π_2, is one, while we reuse the sensing regions of two sensors that have already been placed. We pick a side of the triangle and add the third sensor so that a new triangle Π_2 is formed. By repeating the process, we place all N available sensors and obtain the sensor placement shown in Fig. 10(b). Note that the triangles are added in such a way that the distances among the intersection regions are maximized.

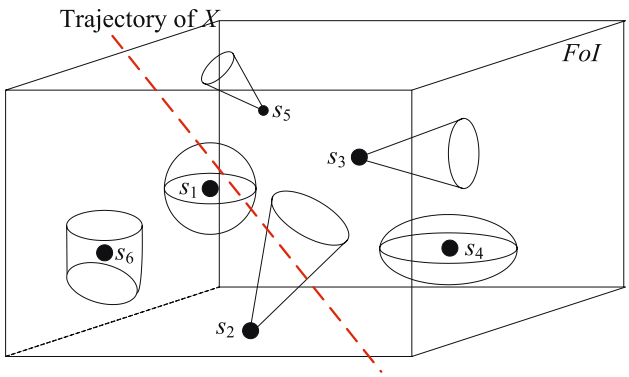

Fig. 11 (**a**) A three-dimensional sensor network. Sensors have sensing regions that can be modeled as three-dimensional rigid bodies. A target X crossing the three-dimensional FoI is detected if it crosses the sensing region of any sensor

5 Deterministic sensor deployment in space

Prior work in target detection in WSN has modeled the sensor networks as planar [2–8, 12–15]. This is due to the fact that most physical targets, such as vehicles and humans, can be assumed to be moving on a plane rather than on the space. However, in certain applications sensors are deployed to detect targets that move in three dimensions and, hence, the sensing regions are three-dimensional rigid bodies. As an example, in underwater sensor networks, sensors are deployed to monitor a three-dimensional volume of water [25–28]. In Fig. 11, we show a three-dimensional sensor network detecting a target X crossing the FoI.

In this section, we analyze the problem of deterministic sensor deployment in space. We compute the target detection probability by at least one sensor P_D as a function of the number of sensors deployed, the relative distance among sensors, and the surface area of the sensing regions of each sensor. First, we derive analytical formulas when only one sensor is deployed within the *FoI*. Then, we extend to the case where two sensors are deployed within the *FoI*, and show the placement of those sensors that maximize P_D. We then generalize for the case of N sensors, and derive relevant lower and upper bounds on P_D, using the cases of one and two sensors as building blocks. Finally, we analyze the problem of collaborative detection in three-dimensional networks.

5.1 Probability of target detection—deployment of a single sensor

Let a single sensor $\mathcal{A}$ be deployed within a three-dimensional *FoI*, $\mathcal{A}_0$. Let also a target X move on a straight line trajectory $\ell(x,y,\Omega)$, where x,y denote the coordinates of the intersection point of the line ℓ with a plane Ω, normal to the direction of the line ℓ. In Fig. 12(a), we show the parameterization of the line ℓ with respect to x, y, Ω.

The probability P_D of detecting the target X crossing the *FoI* can be derived using the same frequency count argument used in Sect. 4.1.1. In Fig. 12(b), we show the "number" of lines crossing the sensing region $\mathcal{A}_0, \mathcal{A}$, and the "number" of lines crossing $\mathcal{A}$, for a fixed trajectory direction θ, in space. Since the set of lines in space intersecting a set $\mathcal{A}$ is uncountable, we use a measure defined in Integral Geometry for the space [20, 29].

Definition 2 Measure of set of lines $m(\ell)$ in space: The measure $m(\ell)$ of a set of lines $\ell(x,y,\Omega)$ is defined as the integral over the line density in space $d\ell = dxdyd\Omega$, $m(\ell) = \int d\ell = \int dxdyd\Omega$.

As in the case of two dimensions, the measure $m(\ell)$ in 3-D is invariant under the set of rigid motions, that is translation, rotation and reflection, yielding the same value for any placement of $\mathcal{A}$ in the space. In the case where $\mathcal{A}$ is convex, the measure of the set of lines that intersect $\mathcal{A}$ is equal to:

$$m(\ell : \ell \bigcap \mathcal{A} \neq \emptyset) = \int_{\ell \bigcap \mathcal{A} \neq \emptyset} dxdyd\Omega = \frac{\pi F}{2}, \tag{28}$$

where F denotes the surface area of $\mathcal{A}$. Interested reader is referred to [20, 29], for the proof of (28). In the case where $\mathcal{A}$ is non-convex, any line intersecting the convex hull of $\mathcal{A}$, also intersects $\mathcal{A}$. Hence, to compute $m(\ell)$ we use the surface area F^h of the convex hull of $\mathcal{A}$. Once we have defined a measure for the set of lines intersecting a set $\mathcal{A}$, the probability of target detection by a single sensor, is given by the quotient of the measure of the set of lines crossing the sensing region of the deployed sensor over the measure of the set of lines crossing the *FoI*.

Proof The proof of Theorem 5 follows the same steps as the proof of Theorem 1 for the two-dimensional case by considering the equivalent measures in 3-D. □

5.2 Probability of target detection—deployment of two sensors

Let two sensors s_i, s_j be deployed anywhere within a three-dimensional *FoI*. The placement of the sensors that maximizes P_D is provided by the following theorem.

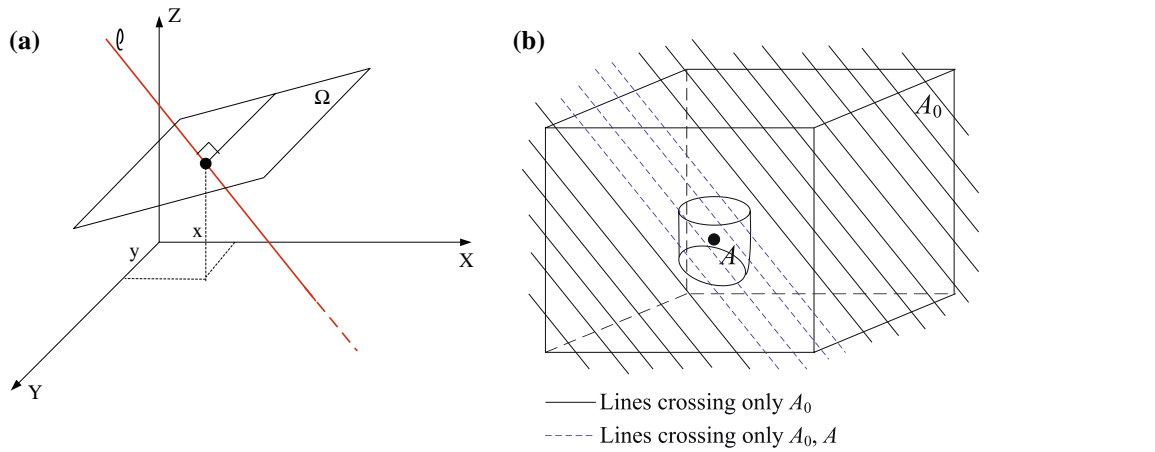

Fig. 12 (**a**) A line $\ell(\xi, \theta)$ on the plane, parameterized by the distance ξ of the line from the origin of the coordinate system, and the angle θ of the line perpendicular to ℓ, with respect to the x-axis. (**b**) The target detection probability P_D as the quotient of the "number" of lines crossing with the *FoI* $\mathcal{A}_0$, over the "number" of lines crossing the sensing region of s $\mathcal{A}$, for a fixed target trajectory θ. The solid lines denote the line that only cross $\mathcal{A}_0$, while the dashed lines denote the lines that cross both $\mathcal{A}_0, \mathcal{A}$, for a fixed target trajectory θ

Theorem 4 *The target detection probability P_D by two sensors s_i, s_j is maximized when s_i, s_j are placed at the opposite ends of the diameter of the FoI, and is given by:*

$$P_D = \frac{F_i + F_j - m_2(d_{i,j})}{F_0}, \tag{29}$$

with

$$m_2(d_{i,j}) = \begin{cases} F_i + F_j - F_{out}(d_{i,j}), & \mathcal{A}_i \bigcap \mathcal{A}_j \neq \emptyset, \\ F_{in}(d_{i,j}) - F_{out}(d_{i,j}), & \mathcal{A}_i \bigcap \mathcal{A}_j = \emptyset, \end{cases} \tag{30}$$

where $d_{i,j}$ denotes the pairwise distance between s_i,s_j, $m_2(d_{i,j})$ denotes the measure of the set of lines intersecting both $\mathcal{A}_i, \mathcal{A}_j, F_{in}(d_{i,j})$ denotes the length of the inner surface area wrapped around $\mathcal{A}_i, \mathcal{A}_j$ as shown in Fig. 13(a), and $F_{out}(d_{i,j})$ denotes the length of the outer surface area wrapped around $\mathcal{A}_i, \mathcal{A}_j$ as shown in Fig. 13(b).

Theorem 5 *The probability that a target X is detected by a sensor s with sensing region $\mathcal{A}$ of surface area F, deployed within a FoI $\mathcal{A}_0$ of surface area F_0 is given by $P_D = \frac{F}{F_0}$.*

Proof The proof of Theorem 4, follows the same steps as the proof of Theorem 2 by considering surfaces instead of lines and, hence, is omitted. □

As in the case of the sensor deployment on the plane, $m_2(d_{i,j})$ is a monotonically decreasing function of the pairwise distance $d_{i,j}$ among the sensors. Thus, the probability of target detection P_D increases with the increase of the pairwise distance $d_{i,j}$ and approaches the asymptotic value of $\frac{F_i+F_j}{F_0}$. Therefore, the sensor constellation that maximizes P_D for the case of two sensors, occurs when the sensors are placed at the opposite ends of the diameter of the *FoI*.

5.3 Probability of target detection—generalization to the deployment of N sensors

When N sensors can be placed within the *FoI*, the probability of detecting a target X is expressed using the inclusion-exclusion principle for unions of sets as in the case of sensor deployment on the plane.

$$P_D = \sum_{i=1}^{N} P(\ell \cap \mathcal{A}_i \neq \emptyset) - \sum_{i,j,i<j} P(\ell \cap \mathcal{A}_i \cap \mathcal{A}_j \neq \emptyset) + \cdots + (-1)^{N+1} P(\ell \cap \mathcal{A}_1 \cap \cdots \cap \mathcal{A}_N \neq \emptyset). \tag{31}$$

While (31) expresses the exact analytic formula for P_D, the number of terms that must be computed is $(2^N - 1)$. Hence, we consider lower and upper bounds for finite unions.

$$\sum_{i=1}^{N} P(\ell \cap \mathcal{A}_i \neq \emptyset) - \sum_{i,j,i<j} P(\ell \cap \mathcal{A}_i \cap \mathcal{A}_j \neq \emptyset) \leq P_D \leq \sum_{i=1}^{N} P(\ell \cap \mathcal{A}_i \neq \emptyset), \tag{32}$$

$$\frac{1}{F_0}\left(\sum_{i=1}^{N} F_i - \sum_{i,j,i<j} m_2(d_{i,j})\right) \leq P_D < \frac{1}{F_0}\sum_{i=1}^{N} F_i. \tag{33}$$

The lower bound approaches the upper bound as the pairwise distances $d_{i,j}$ among each pair of sensors increase. This is a consequence of the asymptotic behavior of P_D for $N = 2$, as we showed in Sect. 5.2. Hence, by increasing the pairwise distance $d_{i,j}$ among each pair of sensors, the lower bound of P_D tends to the upper bound and P_D attains its maximum value. Given the complexity of (31) and the asymptotic behavior of P_D, in the following section we consider the optimization of the lower bound of P_D.

5.4 Analogy of target detection to three-dimensional digital modulation schemes

In the three-dimensional case, the problem of finding the sensor constellation that maximizes the lower bound in (33) is analogous to the problem of finding a three-dimensional signal constellation that minimizes the average probability of symbol error P_{SE}, over an AWGN channel. As in the case of two-dimensional constellations, the average probability of symbol error is minimized when the pairwise distance among the symbols in the three-dimensional space is maximized [22]. The problem of maximizing the minimum pairwise distance among points in space, can be addressed using the following sphere packing problem as an intermediate step [23]. *Given N spheres C_i, $i = 1,\ldots, N$, compute the maximum radius of*

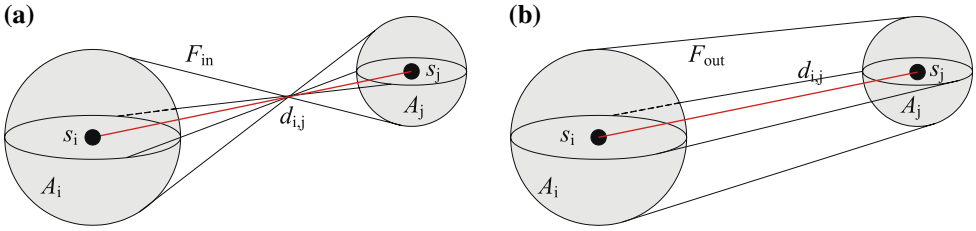

Fig. 13 (**a**) The inner surface F_{in} wrapped around the three-dimensional sensing regions of sensors s_i, s_j, located at a distance $d_{i,j}$ (**b**) The outer surface F_{out} wrapped around the three-dimensional sensing regions of the sensors s_i, s_j

the spheres that would fit inside a given three-dimensional set $\mathcal{A}_0$.

The sphere packing problem, has known optimal solutions for small values of N, and certain shapes of *FoI*, such as sphere, cube, or hexagonal polyhedron, but no optimal solutions exist for large N [22–24]. However, good signal constellations can be carved from lattices with high sphere packing density [23]. In order to place sensors within a three-dimensional *FoI*, we execute to our heuristic for the planar case

Step 1: Fit N spheres $C_i(r)$, $i = 1,\ldots, N$ of equal radius r within the *FoI* so that the radius r is maximized (solution to the sphere packing problem).
Step 2: For each sphere $C_i(r)$ of the constellation, if C_i is on the perimeter of the *FoI*, place the sensor s_i within C_i so that the sensing region $\mathcal{A}_i$ is tangential to the perimeter of $\mathcal{A}_0$.
Step 3: If sphere C_i is an inner circle (not tangent to the perimeter of the *FoI*), place the sensor s_i within C_i so that the sensing region $\mathcal{A}_i$ is centered to the center of C_i.

In Fig. 14(a), we show the optimal placement of N spheres within a spherical *FoI* that maximizes the radius of the N spheres [23]. In Fig. 14(b), we show the placement of N spherical sensing regions within each of the N spheres of Fig. 14(a), according to the sphere placement of Fig. 14(a).

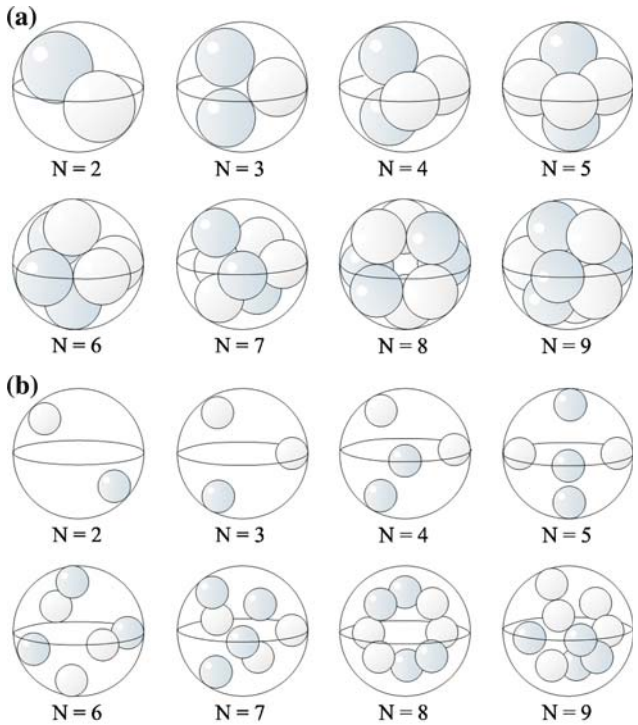

Fig. 14 (**a**) The optimal placement of N spheres within a spherical *FoI* that maximizes the radius of the N spheres. (**b**) The placement of N spherical sensing regions within each of the N spheres of Fig. 14(a) so that the minimum pairwise distance among the sensors is maximized

When the optimal solution of the sphere packing problem is utilized by our heuristic, the minimum pairwise distance among the sensors is maximized.

5.5 Collaborative target detection in space

5.5.1 *Collaborative target detection by* k *sensors*

Let us consider the case where we want to collaboratively detect a target X, in space. To achieve collaborative detection by k sensors, the target X has to cross the intersection of k three-dimensional sensing regions. Hence, in the case of collaborative detection, the sensing regions of k sensors have to be placed in such a way that $\mathcal{A}_1,\ldots\mathcal{A}_k$, intersect.

As in the case of planar WSN, since $\mathcal{A}_1,\ldots\mathcal{A}_k$, are closed and bounded sets, their intersection $\mathcal{A}_c$ is also a closed and bounded set. Let P_c denote the probability that a random line crosses the intersection region $\mathcal{A}_c$. Based on Theorem 5, the probability P_c is a monotonically increasing function of the surface area of $\mathcal{A}_c, F_c$. Let the perimeter F_c of the intersection region $\mathcal{A}_c$ be expressed as a function of the pairwise distances $d_{i,j}$ between the sensors, and let also the correlation function given by (1). The probability of collaborative detection C_D by the k-tuple of sensors is a multivariate function, similar to (23):

$$C_D = \left(1 - \rho(d_{1,2}, d_{1,3}, \ldots, d_{k-1,k})\right) \frac{F_c(d_{1,2}, d_{1,3}, \ldots, d_{k-1,k})}{F_0}. \tag{34}$$

When sensors with heterogeneous sensing regions are considered, it may not be feasible to obtain a closed analytical form expressing the surface area F_c. In such a case, the optimization of C_D can be done numerically by considering a quantized version of all possible pairwise distances among the sensors under consideration. Note that for the majority of sensor applications, k is expected to be a small number, and hence, an exhaustive quantized search can be performed before deployment, to determine the k-sensor constellation that optimizes C_D.

5.6 Collaborative detection by k sensors—deployment of N sensors

Let $N > k$ sensors be available for placement within a three-dimensional *FoI*, and let k of them be sufficient for the collaborative detection of the target X. For any sensor constellation, the probability of target detection is characterized by the number and relative distance of the distinct intersection regions $\mathcal{A}_{c_i}$ formed by the intersection of k sensors. Once the sensors are placed within the *FoI*, the collaborative detection probability C_D is given by (31). That is,

$$C_D = \sum_{i=1}^{N} P(\ell \cap \mathcal{A}_{c_i} \neq \emptyset) - \sum_{i,j,i<j} P(\ell \cap \mathcal{A}_{c_i} \cap \mathcal{A}_{c_j} \neq \emptyset) + \cdots + (-1)^{N+1} P(\ell \cap \mathcal{A}_{c_1} \cap \cdots \cap \mathcal{A}_{c_{N-1}} \neq \emptyset), \quad (35)$$

where the sensing regions $\mathcal{A}_i$ of Theorem 3 have now been substituted by the intersection regions $\mathcal{A}_{c_i}$ of k sensing regions. As we showed in Sect. 5.3, the number of terms in (25) grows exponentially with the network size and not all terms can be analytically computed. Hence, we derived lower and upper bounds for the probability of target detection. Similarly, lower and upper bounds can be derived for the probability of collaborative detection C_D.

$$\sum_{i=1}^{N} P(\ell \cap \mathcal{A}_{c_i} \neq \emptyset) - \sum_{i,j,i<j} P(\ell \cap \mathcal{A}_{c_i} \cap \mathcal{A}_{c_j} \neq \emptyset) \leq C_D \leq \sum_{i=1}^{N} P(\ell \cap \mathcal{A}_{c_i} \neq \emptyset). \quad (36)$$

For the placement of the sensors within the *FoI* for the case of three-dimensional networks we use the same heuristic algorithm presented in Sect. 4.3. The only difference for the three-dimensional case is that the sensors can be placed in the vertices of a k-polyhedron rather than a k-polygon. However, we still follow the main principle of generating $(k-1)$-connected networks, as illustrated in Sect. 4.3, where each node of the network has the minimum possible degree.

6 Performance evaluation

In this section we evaluate the performance of our heuristics with respect to other sensor placement solutions such as random deployment. We also illustrate the impact of network parameters such as number of sensors deployed, length of perimeters and size of surface areas of sensing regions.

6.1 Methodology

We first deployed N sensor nodes within the *FoI* according to a predefined algorithm such as one of our heuristics or randomly. For each network instance, we generated 10,000 random target trajectories and measured the fraction of trajectories that intersect with the sensing region of one or more sensors. For deterministic deployments one trial was sufficient to statistically estimate the target detection probability, since the placement of the sensors does not change over trials and a sufficient number of trajectories are considered to guarantee statistical validity. For random deployments, we repeated the experiment for 100 network deployments in order to compute the average target detection probability.

We initially considered homogeneous WSN where all nodes had identical sensing regions. The experiments for the homogeneous case provide an easy interpretation of the behavior of P_D with respect to network parameters. We then performed our experiments in heterogeneous WSN. To simulate heterogeneous WSN, we generated a pool of sensing regions of different shapes (circle, square, triangle, pentagon, hexagon and equivalent three-dimensional shapes) and randomly selected N to be placed within the *FoI*.

6.2 Probability of target detection for homogeneous WSN

6.2.1 Sensor deployment on the plane

In our first experiment, we placed $N = 2,\ldots, 9$ sensors in a circular *FoI* of radius $R = 100$ m, according to the WSN constellations shown in Fig. 7(a). Sensors had identical sensing ranges that varied from $r = 5$ m to $r = 20$ m. We measured the target detection probability P_D and also computed the analytical lower bound given by (15). In Fig. 15(a), we show the target detection probability P_D vs. the number of sensors deployed for varying r and the corresponding lower bound.

We observe that for small values of r ($r = 5$ m, 10 m) the lower bound provides a very good estimate of the actual value of P_D. This is due to the fact that no lines intersect more than two sensing regions. Hence, the lower bound in (15) that takes into account only lines that intersect one or two sensing regions is exact. Furthermore, we observe that for small values of r the P_D increases almost linearly with the number of sensors deployed. This is due to the fact that the measure $m_2(d_{i,j})$ of lines that intersect two sensing regions is very small when the pairwise distance among the sensors is sufficiently large compared to their sensing range. This is illustrated in Fig. 3(b) where we show that when $d_{i,j} = 20r$ the probability that a line intersects two sensing regions is almost negligible. Hence, for these values of r, the lower bound approaches the upper bound and P_D is maximized.

For larger values of sensing range r and WSN values of $N \geq 6$ we observe that the lower bound starts to deviate from the probability of detection P_D. In fact, the lower bound starts to decrease with the increase of N. This is due to the fact that for large values of r and N, the probability that a line would intersect three or more sensing regions is non-negligible and hence, omitting this additive factor from the lower bounds yields its deviation from the true value of P_D.

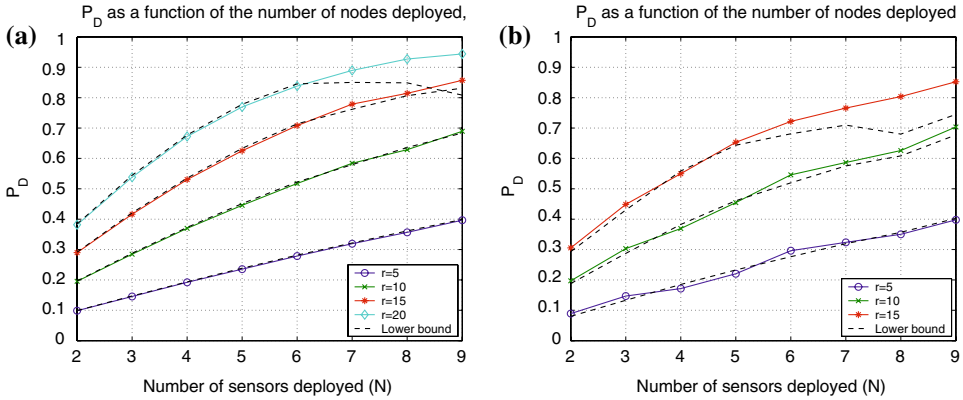

Fig. 15 The target detection probability P_D as a function of the number of sensors deployed and the sensing range radius r for the sensor constellations of, (**a**) Fig. 7(a), (**b**) Fig. 7(b)

In Fig. 15(b), we show the target detection probability P_D for the WSN constellations shown in Fig. 7(b). The *FoI* is now a square with each side being $\alpha = 100$ m. Again we observe that for small values of r the lower bound is very tight to the value of P_D obtained via the simulation, while the lower bound deviates from P_D for large values of r, N.

In our second experiment, we compared the target detection probability achieved by our heuristic with the target detection probability achieved by random sensor deployment. Although this comparison is unfair since random deployments yield lower performance due to overlapping sensing regions, it is an indicator of the performance gains that can be achieved by adopting a deterministic solution. For each value of N we randomly deployed the N sensors within the *FoI* and measured P_D. We repeated the same experiment 100 times and averaged the result. In Fig. 16(a), we show the target detection probability for $N = 2,\ldots, 40$ and for a sensing range $r = 5$ m. We observe the our placement algorithm yields a performance gain up to 14% compared to random deployment (average case), while random deployment can yield WSN constellations that are up to 90% worse.

In Fig. 16(b), we show P_D for $N = 2,\ldots, 14$ and for a sensing range $r = 20$ m. For $r = 20$ m we considered WSN of smaller sizes since larger WSN would be able to entirely cover the boundary of the *FoI* thus yielding a $P_D = 1$. We observe that for sensing regions of larger perimeter, the gains are even greater, due to the higher sensing region overlap in random deployments. Our heuristic yields a P_D up to 18% higher, on average, compared to the performance of the random deployment.

The benefits of adopting our placement strategy are even more significant, when the savings in number of sensors is considered. From Fig. 16(a), we observe that we requires 26 sensors to achieve a target detection probability of $P_D = 0.8$. On the other hand, 40 sensors are required to achieve the same target detection probability using random deployment, that is, 54% more sensors are required in the random deployment case. Similarly, from Fig. 16(b), we observe that we need to place only five sensors to achieve a target detection probability of $P_D = 0.78$. On the other hand, 11 sensors are required to achieve the same target detection probability using random deployment, that is, 120% more sensors are required in the random deployment case.

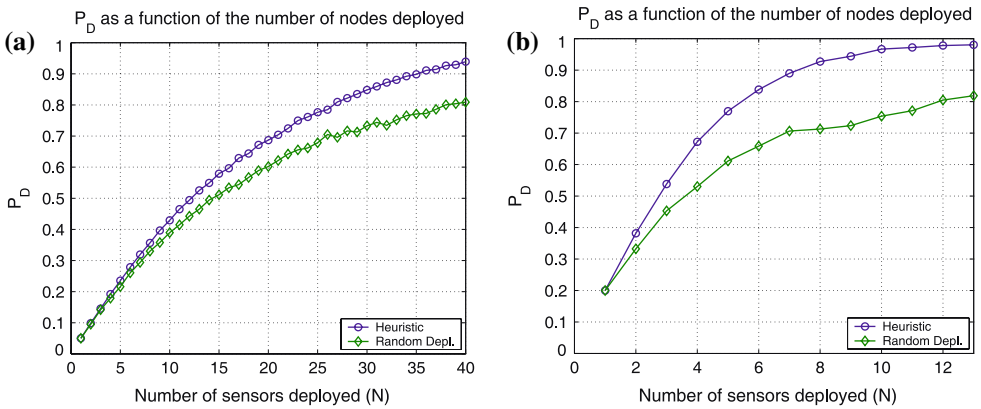

Fig. 16 Comparison of the performance of our heuristic vs. random deployment for homogeneous WSN with sensing range (**a**) $r = 5$ m, (**b**) $r = 20$ m

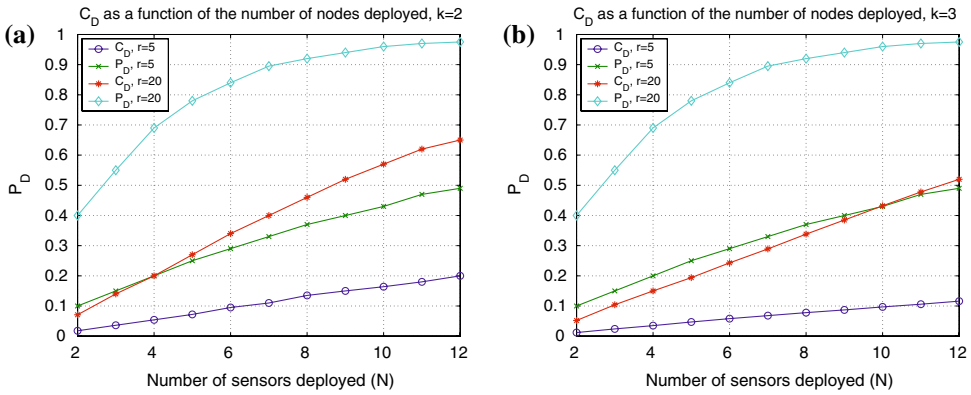

Fig. 17 The probability of collaborative target detection on the plane, as a function of the number of sensors deployed for (**a**) $k = 2$, (**b**) $k = 3$

6.2.2 *Sensor deployment on the plane—collaborative detection*

For the case of collaborative detection, we placed N sensors in a circular *FoI* of radius $R = 100$ m, according to the WSN constellations shown in Figs. 10(a) and (b). Sensors had identical sensing ranges of $r = 5$ m, and $r = 20$ m. We measured the probability of collaborative detection C_D and compared it with the probability of detection P_D by a single sensor. In Fig. 17(a) and (b), we show the probability of collaborative target detection C_D, for $k = 2,3$, respectively, and the probability of detection by a singe sensor vs. the number of sensors deployed.

We observe that the probability of collaborative target detection is significantly smaller than the probability of detecting the target by any individual sensor. This is due to the fact that the length of the perimeters of the intersection regions $\mathcal{A}_{c_i}$ is significantly smaller than the perimeter of each individual sensor. Furthermore, the observations from sensors whose sensing regions overlap are correlated and, hence, the fidelity of the detection is reduced by the application of the correlation function in (1). Finally, in the collaborative detection case, sensors have to be placed close enough so that their sensing regions overlap, thus also bringing the intersection regions to close proximity. As a result the measure of the set of lines intersecting more than one $\mathcal{A}_{c_i}$ is significant, leading C_D away from its upper bound. On the other hand, in the probability of detection by a single sensor, the sensing regions can be placed arbitrarily far away within the limits of the *FoI*.

6.2.3 *Sensor deployment in space*

For our experiments in space, we placed N sensors in a spherical *FoI* of radius $R = 100$ m, according to the WSN constellations shown in Fig. 14(b). Sensors had identical sensing ranges that varied from $r = 5$ *m* to $r = 20$ m. We measured the target detection probability P_D and also computed the analytical lower bound given by (36). In Fig. 18(a), we show the target detection probability P_D vs. the number of sensors deployed for varying r and the corresponding lower bound.

We observe that for values of $r = 5$ m, 10 m 15 m, the lower bound provides a very good estimate of the actual value of P_D. This is due to the fact that no lines intersect more than two sensing regions, and the lower bound in (36) is exact. We also observe that the probability of target detection in space is significantly smaller than the probability of detection achieved by the deployment of same number of sensors (same radius) on the plane. This can be interpreted by noting that for spherical (circular) sensing

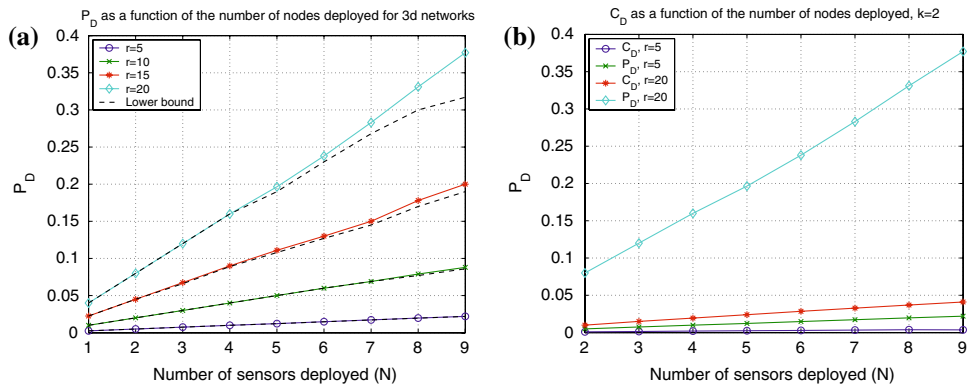

Fig. 18 (**a**) The target detection probability P_D as a function of the number of sensors deployed and the sensing range radius r for the sensor constellations of Fig. 14(b). (**b**) The collaborative target detection probability for $k = 2$, as a function of the number of sensors deployed for the case of three-dimensional *FoI*. Comparison with the probability of detection by a single sensor

regions, the probability of target detection by the deployment of single sensor in space is the square of the probability of target detection by the deployment of a single sensor on the plane. Given that $P_D \leq 1$ the probability of target detection in space is smaller than that on the plane.

We also evaluated the probability of collaborative target detection C_D in space, by deploying sensors with three-dimensional sensing regions within a spherical *FoI*, according to the heuristic algorithm described in Sect. 4.3. In Fig. 18(b), we show C_D as a function of the number of sensors deployed for $r = 5$ m and $r = 20$ m, and for $k = 2$. We also compare the C_D with the probability of target detection by a single sensor P_D. As in the case of collaborative detection on the plane, we observe that requiring collaborative detection of the target reduces the probability of detection compared to target detection by a single sensor.

6.3 Target detection probability for heterogeneous WSN

For the case of heterogeneous WSN, we repeated the experiments we conducted for the homogeneous case by placing nodes with heterogeneous sensing regions. The shape and size of the sensing regions were randomly selected from a pool of five shapes (circular, square, triangle, pentagon, hexagon). In Fig. 19, we show the target detection probability for WSN of different sizes and as a function of the sensing range r. For the heterogeneous WSN case, the sensing range denotes a circle where the sensing region of each sensor can be inscribed. As an example when the sensing region of the selected node is square, the side of the sensing region is equal to $\alpha = \sqrt{(2)}r$, and its perimeter equal to $L_i = 4\sqrt{(2)}r$.

We observe that in the heterogeneous case, the lower bound still accurately predicts the target probability of detection when the sensing range is small. For higher values of r the lower bound deviates from P_D indicating that a significant number of lines intersect with more than two sensing regions. Also, compared to the homogeneous case, the target detection probability does not exhibit a linear behavior. This is due to the fact that the perimeters of the sensing regions are no longer constant, but vary with the shape of the sensing regions.

We also repeated the comparison of our placement algorithm with a random sensor deployment strategy, for heterogeneous WSN. In Fig. 20, we show the target detection probability as a function of the WSN size. As expected, our placement algorithm performs better than the random deployment strategy, with the difference in performance increasing as the number of sensors deployed also increases. Regardless of the shapes of the sensing regions and the lengths of the perimeters, random deployment can result in overlapping sensing regions and sensors with constellations with small pairwise distances, thus having inferior performance to deterministic deployment.

7 Conclusion

We addressed the problem of deterministic deployment of WSN for maximizing the target detection probability in planar and three-dimensional networks. We considered the metrics of probability of detection by at least one sensor and collaborative detection by k sensors. We derived analytic formulas expressing the probability of detection by mapping the target detection problem to the line-set intersection problem. Our formulation allowed the consideration of WSN with heterogeneous sensing capabilities. We showed that the analytic expressions of P_D are not practical for large N and derived lower and upper bounds. We finally showed that maximizing the lower bound, is analogous to minimizing the average symbol error probability in two and three-dimensional modulation schemes, over an AWGN channel for the plane and space respectively, and derived WSN constellations from well known signal constellations.

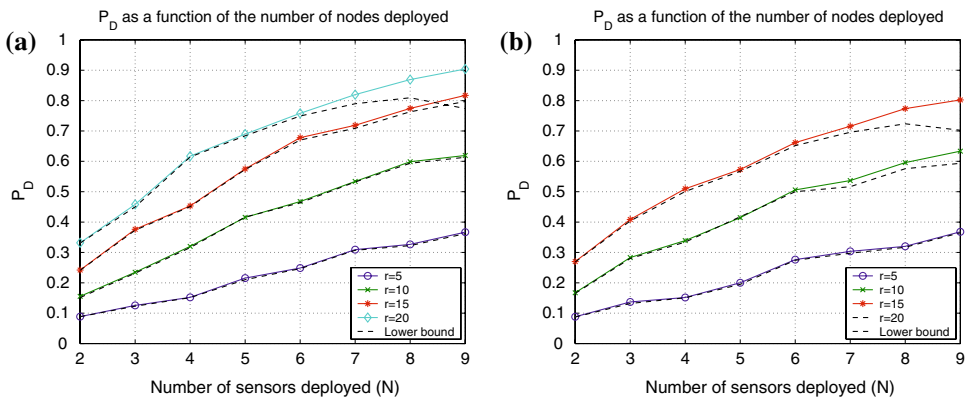

Fig. 19 The target detection probability P_D as a function of the number of sensors deployed and the sensing range radius r for the sensor constellations of, (**a**) Fig. 7(a), (**b**) Fig. 7(b). The sensors deployed have heterogeneous sensing capabilities

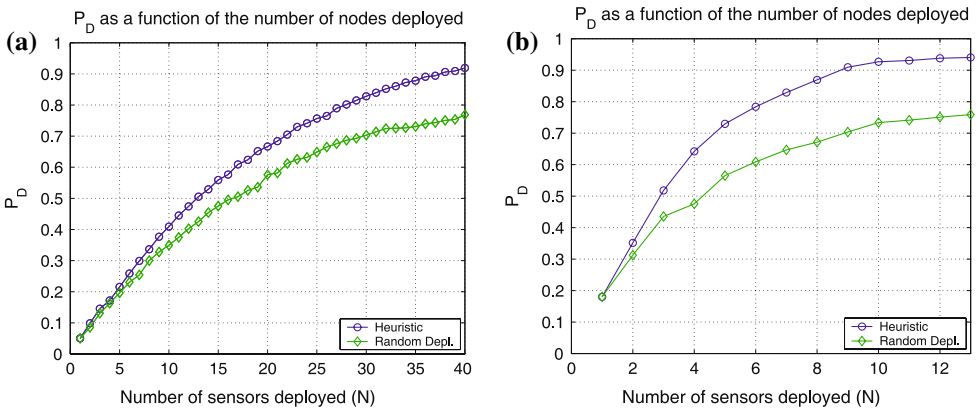

Fig. 20 Comparison of the performance of our heuristic vs. random deployment for heterogeneous WSN with sensing range (**a**) $r = 5$ m, (**b**) $r = 20$ m

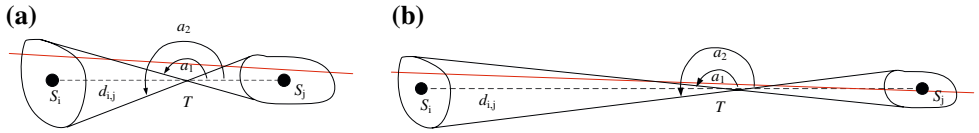

Fig. 21 (**a**) Any line intersecting both sensing areas has a slope $a_1 \leq a \leq a_2$, (**b**) when $d_{i,j}$ increases, the slope difference $a_2 - a_1$ decreases and, hence, a smaller number of lines intersects both sensing areas. Therefore, the measure $m_2(d_{i,j})$ of the set of lines intersecting two sensing areas is a monotonically decreasing function of $d_{i,j}$

Acknowledgments This work was supported in part by the following grants: ONR YIP award, N00014-04-1-0479, ARO PECASE grant, W911NF-05-1-0491, ARL CTA Grant DAAD 19-01-2-0011, and ARO MURI Grant #W 911 NF 0710287. This document was prepared through collaborative participation in the Communications and Networks Consortium sponsored by the US Army Research Laboratory under the Collaborative Technology Alliance Program, DAAD19-01-2-0011. The US Government is authorized to reproduce and distribute reprints for Government purposes notwithstanding any copyright notation thereon. The views and conclusions contained in this document are those of the author and should not be interpreted as representing the official policies, either expressed or implied, of the Army Research Laboratory or the US Government.

Appendix

In this section, we prove the monotonicity of $m_2(d_{i,j})$ as it is expressed in Corollary 1.

Proof To prove the monotonicity of $m_2(d_{i,j})$, we must show that $m_2(d_{i,j})$ becomes smaller as the distance $d_{i,j}$ among the sensing area $\mathcal{A}_i, \mathcal{A}_j$ increases. For cases where L_{in}, L_{out} have an analytical form, this can be easily shown by computing the first derivative of $(L_{in} - L_{out})$, with respect to $d_{i,j}$. As an example, when the two sensing areas are discs of radius r, we can analytically express L_{in}, L_{out} as follows:

$$L_{in} = 2\left(\pi r + arc\tan\left(\frac{2r}{d_{i,j}}\right)r + 2\sqrt{\frac{d_{i,j}^2}{4} - r^2}\right),$$
$$L_{out} = 2(\pi r + d_{i,j}). \tag{37}$$

Computation of the derivative of $(L_{in} - L_{out})$ verifies the monotonicity of $m_2(d_{i,j})$ (this is an elementary mathematic exercise not presented here due to space constraints). For the case where $(L_{in} - L_{out})$ does not have a closed analytic form, we can illustrate the monotonicity of $m_2(d_{i,j})$ by considering its equivalence to the set of lines intersecting both sets. The argument in our proof is that as $d_{i,j}$ increases, a smaller "number" of lines will intersect both sets and, hence, $m_2(d_{i,j})$ becomes smaller.

Let a_1, a_2 denote the slopes of the lines of the inner string that wraps around $\mathcal{A}_i, \mathcal{A}_j$, as shown in Fig. 21(a). Any line that is crossing both $\mathcal{A}_i, \mathcal{A}_j$ must have a slope a with $a_1 \leq a \leq a_2$. As an example, all lines that pass through the intersection point T with slope $a_1 \leq a \leq a_2$ intersect both sensing areas. The measure of the set of lines crossing both sensing areas is monotonically related to the range of $(a_2 - a_1)$ that is the greater the difference between the slopes a_1, a_2 the larger the "number" (measure) of lines that cross both sets (more lines out of all possible trajectories satisfy the $a_1 \leq a \leq a_2$ condition).

As the distance $d_{i,j}$ between the sets $\mathcal{A}_i, \mathcal{A}_j$ increases, the slope difference $(a_2 - a_1)$ decreases and, hence the "number" of lines intersecting both sets also decreases. Therefore, $m_2(d_{i,j})$ which expresses the measure of the set of lines intersecting both sensing areas, also decreases with the decrease of the slope difference, or equivalently with the increase of the pairwise distance $d_{i,j}$. In Fig. 21(b), we show the reduction in the slope difference $(a_2 - a_1)$ that reduces the set of lines that intersect both sets. □

References

1. Akyildiz, I. F., Su, W., Sankarasubramaniam, Y., & Cayirci, E. (2002). A survey on sensor networks. *IEEE Communications Magazine, 40*(8), 102–116.
2. Aslam, J., Butler, Z., Constantin, F., Crespi, V., Cybenko, G., & Rus, D. (2005). Tracking a moving object with a binary sensor

network. In *Proceedings of the 1st International Conference on Embedded Networked Sensor Systems*, Nov. 2005, pp. 150–161.
3. Cao, Q., Yan, T., Abdelzaher, T., & Stankovic, J. (2005). Analysis of target detection performance for wireless sensor networks. In *Proceedings of the International Conference on Distributed Computing in Sensor Networks*, CA, Jun. 2005.
4. Chakrabarty, K., Iyengar, S., Qi, H., & Cho, E. (2002). Grid coverage for surveillance and target location in distributed sensor networks. *IEEE Transactions on Computers, 51*, 1448–1453.
5. Clouqueur, T., Phipatanasuphorn, V., Ramanathan, P., & Saluja, K. K. (2002). Sensor deployment strategy for target detection. In *Proceedings of the 1st ACM International Workshop on Wireless Sensor Networks and Applications*, pp. 42–48.
6. Dousse, O., Tavoularis, C., & Thiran, P. (2006). Delay of intrusion detection in wireless sensor networks. In *Proceedings of Mobihoc* 2006.
7. Gui, C., & Mohapatra, P. (2004). Power conservation and quality of surveillance in target tracking sensor networks. In *Proceedings of the 10th Annual International Conference on Mobile Computing and Networking*, Sep. 2004, pp. 129–143.
8. Meguerdichian, S., Koushanfar, F., Qu, G., & Potkonjak, M. (2001). Exposure in wireless ad hoc sensor networks. In *Proceedings of MOBICOM 2001*, Jul. 2001, pp. 139–150.
9. Harter, A., & Hooper, A. (1997). A new location technique for the active office. *IEEE Personal Communications, 4*(5), 42–47.
10. Savvides, A., Han, C. C., & Strivastava, M. B. (2001). Dynamic fine-grained localization in ad-hoc networks of sensors. In *Proceedings of the 7th Annual International Conference on Mobile Computing and Networking (MOBICOM), 2001*, pp. 166–179.
11. Koushanfar, F., Slijepcevic, S., Potkonjak, M., & Sangiovanni-Vincentelli, A. (2002). Error-tolerant multimodal sensor fusion. In *Proceedings of IEEE CAS Workshop on Wireless Communication and Networking*.
12. Kumar, S., Lai, T. H., & Arora, A. (2005). Barrier coverage with wireless sensors. *In Proceedings of the 11th Annual International Conference on Mobile Computing and Networking (MobiCom '05)*, 2005, pp. 284–298.
13. Lazos, L., Poovendran, R., & Ritcey, J. A. (2007). Probabilistic detection of mobile targets in heterogeneous sensor networks. In *Proceedings of the 6th International Symposium on Information Processing in Sensor Networks*, (IPSN '07), 2007, pp. 519–528.
14. Lazos, L., Poovendran, R., & Ritcey, J. A. (2007). On the deployment of heterogeneous sensor networks for detection of mobile targets. *In Proceedings of the 5th International Symposium on Modeling and Optimization in Mobile, Ad Hoc and Wireless Networks*, (WiOpt '07), 2007.
15. Yang, H., & Sikdar, B. (2003). A protocol for tracking mobile targets using sensor networks. In *Proceedings of the First IEEE 2003 International Workshop on Sensor Network Protocols and Applications*, pp. 71–81.
16. Li, D., Wong, K., Hu, Y. H., & Sayeed, A. M. (2002). Detection, classification, and tracking of targets in distributed sensor networks. *Signal Processing Magazine, IEEE, 19*(2), 17–29.
17. Akyildiz, I. F., Vuran, M. C., & Akan, O. B. (2004). On exploiting spatial and temporal correlation in wireless sensor networks. In Proceedings of *WiOpt'04*, pp. 71–80, Mar. 2004.
18. Santalo, L. A. (1976). *Integral geometry and geometric probability*. Addison-Wesley Publishing Company.
19. Sylvester, J. (1890). On a funicular solution of Buffon's needle problem. *Acta Mathematica, 14*, 185–205.
20. Deltheil, R. (1926) Probabilités Géométriques. París.
21. Feller, W. *An introduction to probability theory and its applications* (3rd ed.). John Wiley and Sons Inc.
22. Benedetto, S., & Biglieri, E. (1999). *Principles of digital transmission with wireless applications*. NY: Kluwer.
23. Conway, J. H., & Sloane, N. J. (1998). *Sphere packings, lattices and groups* (3rd ed.). NY: Springer-Verlag.
24. Boutros, J., Viterbo, E., Rastello, C., & Belfiore, J. (1996). Good lattice vonstellations for both Rayleigh fading and Gaussian Channels. *IEEE Transactions on Information Theory, 42*(2), 502–518.
25. Akyildiz, I. F., Pompili, D., & Melodia, T. (2005). Underwater acoustic sensor networks: Research challenges. *Ad Hoc Networks (Elsevier), 3*(3), 257–279.
26. Pompili, D., Melodia, T., & Akyildiz, I. F. (2006). Deployment analysis in underwater acoustic wireless sensor networks. In *Proceedings of ACM International Workshop on UnderWater Networks (WUWNet)*, Los Angeles, CA, Sep. 2006.
27. Ravelomanana, V. (2004). Extremal properties of three-dimensional sensor networks with applications. *IEEE Transactions on Mobile Computing, 3*(3), 246–257.
28. Cayirci, E., Tezcan, H., Dogan, Y., & Coskun, V. (2004). Wireless sensor networks for underwater surveillance systems. *Ad Hoc Networks*, in press; doi:10.1016/j.adhoc.2004.10.008.
29. Santalo, L. A. (1943). Sobre La Distribución Probable de Corpúsculos en un Cuerpo, Deducida de la Distribución en sus Secbiones y Problemas Análogos. *Revista de la Unión Matemática Argentina, 9*, 145–164.

Author Biographies

Loukas Lazos received his B.S. degree from the National Technical University of Athens, Greece, his M.S. and Ph.D. degrees from the University of Washington. Since 2007, he is an Assistant Professor of Electrical and Computer Engineering at the University of Arizona. He was the Co-director of the Network Security Laboratory at the University of Washington, until July 2007. His research interests are in the areas of networking and distributed systems, focusing on the identification, modeling and mitigation of network security vulnerabilities in wireless networks and analysis of network performance.

Radha Poovendran is an Associate Professor and founding director of the Network Security Lab (NSL) at the Electrical Engineering Department of the University of Washington. He received his Ph.D. in Electrical Engineering from the University of Maryland, College Park in 1999. His research interests are in the areas of applied cryptography for multiuser environment, wireless networking, and applications of Information Theory to security. He is a recipient of the NSA Rising Star Award and Faculty Early Career Awards including NSF CAREER (2001), ARO YIP (2002), ONR YIP (2004), and PECASE (2005) for his research contributions to multiuser security, the Graduate Mentor Recognition Award from the University of California San Diego in 2006, and is

invited to the Kavli Frontiers of Science Symposium organized by the National Academy of Sciences in 2007. He is a co-editor of the Springer Verlag book "Secure localization and time synchronization in wireless ad hoc and sensor networks."

James A. Ritcey received the BSE degree from Duke University, the MSEE degree from Syracuse University, and the Ph.D. degree in Electrical Engineering (communication theory and systems) from the University of California, San Diego in 1985. Since 1985, he has been with the Department of Electrical Engineering at the University of Washington, where he now holds the rank of Professor. From 1976 to 1981 he was with the General Electric Company, and graduated from GE's Advanced Course in Engineering. His research interests include communications and statistical signal processing for radar and underwater acoustics. He has published extensively in these areas. Professor Ritcey served as the General Chair of the 1995 International Conference on Communications in Seattle. He also served as Technical Program Chair of the 1992 and General Chair of the 1994 Asilomar Conference on Signals, Systems, and Computers and is currently a member of the Steering Committee.